AD-784 137

A NUCLEONIC OIL DEBRIS MONITOR
FOR DETECTING METAL IN RECIRCULATING
LUBRICATING SYSTEMS

Randall W. Harman

Nucleonic Data Systems, Incorporated

EUSTIS DIRECTORATE POSITION STATEMENT

This report is basically an extension and continuation of the work previously conducted under Contract DAAJ02-71-C-0019.

Under the earlier contract, NDS established the feasibility of radioactive sensing of metallic debris in lubricating oil. The objective of the work reported herein was to fabricate two oil debris monitors for test and evaluation by the Government in conjunction with test cell testing of a UH-1 main transmission and a 90° gearbox.

The contractor satisfactorily met the objectives of the program.

The technical monitor for this contract was Mr. R. J. Hunthausen of the Reliability and Maintainability Technical Area, Military Operations Technology Division.

REPORT DOCUMENTATION PAGE		READ INSTRUCTIONS BEFORE COMPLETING FORM
1. REPORT NUMBER USAAMRDL-TR-74-28	2. GOVT ACCESSION NO.	3. RECIPIENT'S CATALOG NUMBER AD-784137
4. TITLE (and Subtitle) A NUCLEONIC OIL DEBRIS MONITOR FOR DETECTING METAL IN RECIRCULATING LUBRICATING SYSTEMS		5. TYPE OF REPORT & PERIOD COVERED Final Report
		6. PERFORMING ORG. REPORT NUMBER
7. AUTHOR(s) Randall W. Harman		8. CONTRACT OR GRANT NUMBER(s) Contract DAAJ02-72-C-0107
9. PERFORMING ORGANIZATION NAME AND ADDRESS Nucleonic Data Systems, Inc. 1821 McGaw Avenue Irvine, Calif. 92705		10. PROGRAM ELEMENT, PROJECT, TASK AREA & WORK UNIT NUMBERS Project 1F262203AH86
11. CONTROLLING OFFICE NAME AND ADDRESS Eustis Directorate, U. S. Army Air Mobility Research and Development Laboratory Fort Eustis, Va. 23604		12. REPORT DATE June 1974
		13. NUMBER OF PAGES 90
14. MONITORING AGENCY NAME & ADDRESS(if different from Controlling Office)		15. SECURITY CLASS. (of this report) Unclassified
		15a. DECLASSIFICATION/DOWNGRADING SCHEDULE

16. DISTRIBUTION STATEMENT (of this Report)

Approved for public release; distribution unlimited.

17. DISTRIBUTION STATEMENT (of the abstract entered in Block 20, if different from Report)

18. SUPPLEMENTARY NOTES

19. KEY WORDS (Continue on reverse side if necessary and identify by block number)

Contamination
Oils
Debris
Monitors
X Rays
Fluorescence

20. ABSTRACT (Continue on reverse side if necessary and identify by block number)

Metallic debris sensors have been developed for recirculating oil lubrication systems. The in-line monitors apply the principle of X-ray fluorescence. The nucleonic oil debris monitors (ODM's) have been designed and fabricated for use with test cell operations involving aircraft transmissions and gearboxes. The ODM is contained in a volume less than 1 cubic foot; it uses a radioactive source to induce X-ray fluorescence.

DD FORM 1473 EDITION OF 1 NOV 65 IS OBSOLETE

Block 20 - contd.

ODM's were tested to evaluate their sensitivity, accuracy, and response to lubricant temperature over the range of 100°F to 300°F. Iron in solution and particles of diameters to 300 microns were used for both dynamic and static tests with MIL-L-7808 oil. Units exhibited a mass sensitivity of less than 4 micrograms (2σ) in a measurement period of approximately 11 minutes. This is equivalent to a uniform mass concentration of approximately 10 ppm. Both debris mass and rate-of-change outputs are provided.

PREFACE

TABLE OF CONTENTS

Preceding page blank

LIST OF ILLUSTRATIONS

LIST OF TABLES

1.0 INTRODUCTION

This report presents information pertaining to the design, development, and testing of advanced nucleonic oil debris monitoring systems. Within these discussions, the nucleonic gauge is given the acronym ODM (i.e., oil debris monitor).

1.1 PROBLEM DEFINITION/BACKGROUND

The quantity of metallic debris in a mechanical system's lubricant is an important indication of the condition of oil wetted components. Quantitative evaluation of specific metallic contaminants can yield diagnostic - and sometimes prognostic - data related to the system's mechanical status.

The purpose of this program was to produce two ODM's for use in testing of aircraft transmissions and gearboxes. No attempt was made to make the units flightworthy since their use was intended for test cell operations.

In a preceding program, gauge technology was developed. During those studies, a laboratory test instrument successfully demonstrated the capability of sensing both particulate and dissolved metal contaminants[1]. The instrument employed a nucleonic gauging method - radioisotope-excited X-Ray Fluorescence (XRF).

1.2 MEASUREMENT TECHNIQUES

The physical phenomenon of XRF is in wide use as a quantitative measurement technique. Gauging equipment employs XRF to measure thickness and density of materials in the metals, papers, and plastics industries. This gauging technique has also been used to measure the concentration of specific elements in a mixture[2,3,4]. As detailed in Reference 1, the principle of XRF was demonstrated to be appropriate in measurements of dissolved and particulate iron in oil. The laboratory instrument detected metal concentrations over the range from 0-550 ppm with an accuracy of less than 6 ppm.

1.3 ODM SYSTEM CONSIDERATIONS

The ODM is intended for on-line sensing of metallic contamination in recirculating oil lubrication systems. Therefore, it is important that the ODM present minimum impedance to fluid flow. Further, the monitor should examine the fluid in a manner such that representative measurements are made (i.e., particles are neither bypassed nor screened, measurement time lag is minimal, etc.). It is important that the ODM be compatible with the designated drive-trains (UH-1 transmission and 90° gearbox).

The gauging instrument design must be appropriate for use in a test cell environment with the capability of unattended operation and remote readout. Simplicity of installation and operation is a desired ODM characteristic.

The factors listed above were major guidelines applied in the efforts to provide units which could easily and reliably measure a metallic contaminant mass as small as 10 micrograms (concentrations ranging from 0-200 ppm).

1.4 PROGRAM SUMMARY

The ODM program involved the selection and testing of specific components which had been generally defined in the previous study. Concurrently, the laboratory instrument design was adapted to this specific application. After assembly of the advanced ODM hardware, system tests were performed.

Significant effort was expended in an unsuccessful attempt to employ a noble gas radionuclide (Krypton-85) as the primary excitation source for XRF. The excessive background radiation (i.e., a poor "signal-to-noise" ratio) and the substantial physical size of the source package resulted in a gauge exhibiting insufficient measurement sensitivity.

ODM's were tested to evaluate measurement sensitivity and accuracy. Additional tests provided data of system response to lubricant temperature over the range from 100° to 300°F. Dynamic and static tests employed MIL-L-7808 oil as the fluid medium. Both iron in solution and particles of diameter to 300 μm were used. Units exhibited a mass sensitivity of less than 4 μg (2σ) in a measurement period of approximately 11 minutes. This is equivalent to a uniform mass concentration of approximately 10 ppm.

Section 2 of this report contains a discussion of X-ray fluorescence theory as applied to the problem of detecting metal in oil. Section 3 details the component and system design studies related to development of the advanced ODM. Section 4 presents data on electromechanical design and configuration of the ODM. Included in Section 4 are data on system operation, calibration and testing. Section 4 also discusses results of program testing. Section 5 contains comments on possible future evolutions of the ODM gauging technique and hardware.

2.0 X-RAY FLUORESCENCE THEORY

Figure 1 is a graphic presentation of the XRF phenomenon. In this illustration, the energy of an incoming photon is absorbed by an electron in the K-shell by the photoelectric effect. The additional energy gained by the electron is sufficient to free it from the Coulomb attraction of the nucleus (i.e., the exciting photon energy is greater than the electron's binding energy). This is shown in Figure 1(a). After the atom has been ionized by the loss of this orbital electron (see Figure 1(b)), its deexcitation process includes the transfer of an L-shell electron to the K-shell (to fill the K-shell vacancy) and the emission of an X-ray photon. Although the processes have been discussed sequentially, the total interaction occurs in less than one femtosecond. In the illustration, the emitted photon is a K X-ray. Its energy is equal to the difference between the K- and L-shell binding energies.

Energy quanta are both unique and discrete for each electron shell of each element. Hence, measurement of X-ray energy permits elemental identification of the atom which emitted the X-ray. Table I presents data related to XRF of likely metallic oil contaminants. Since the overwhelming majority of fluorescence occurs in the K-shell, the data in Table I relates only to K-shell XRF. The fluorescence yield data indicates that decimal fraction of photoelectric interactions which result in the emission of K X-ray. The remaining fraction of photoelectric interactions results in the emission of Auger electrons. (Emission of Auger electrons is another form of atomic deexcitation.) Although the fluorescent X-ray and the Auger electron have comparable energy, the charge and mass of the latter prevent its use in this gauging application.

Another factor which influences XRF of a specific element relates to the probability that a photoelectric interaction will occur. For each small sample thickness increment, this factor is directly proportional to the number of atoms of that element present and the number of excitation source photons available for the interaction. Since the atomic number is proportional to the electron population of the atom, one can expect greater photon absorption in iron atoms (Z = 26) than in aluminum atoms (Z = 13). The process is roughly proportional to the fourth power of Z. In a given sample thickness, photon absorption rate decreases as photon energy increases.

In Figure 2 the mass absorption coefficient (μ/ρ) of various elements is presented as a function of excitation photon energy.

3
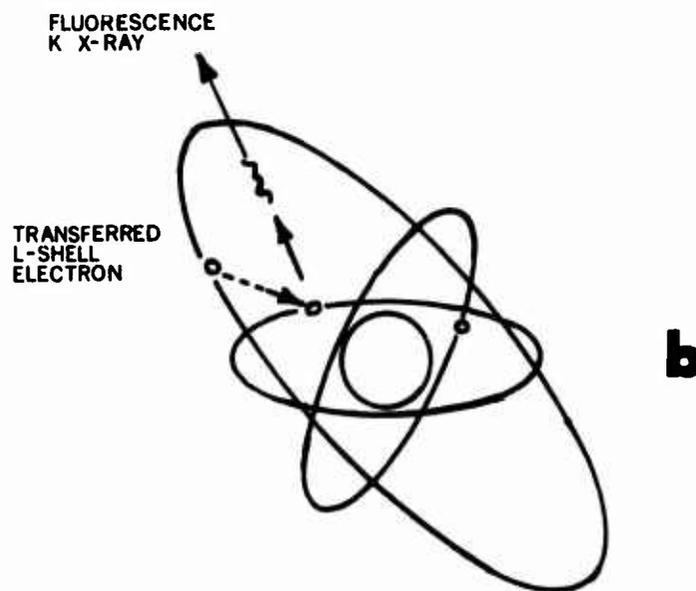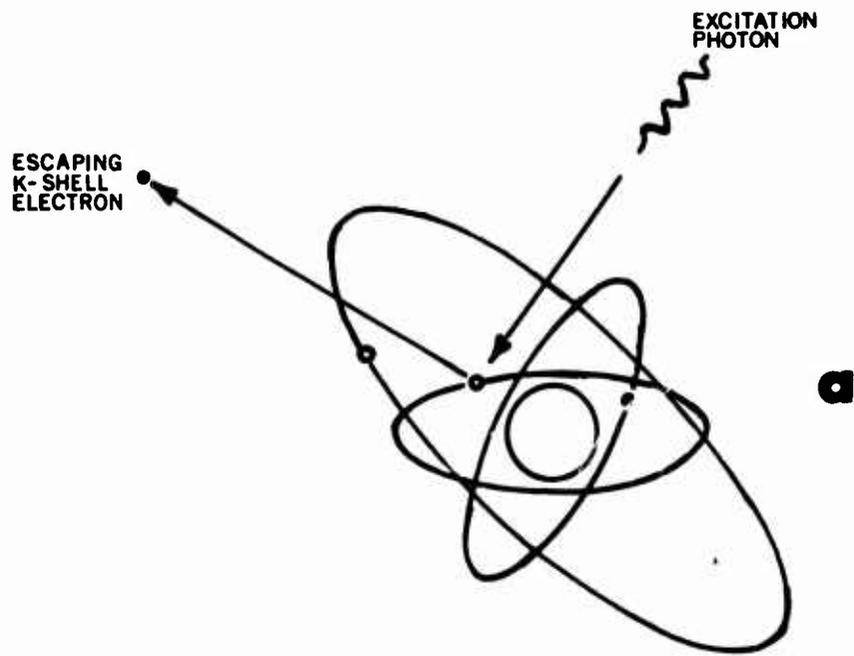
Figure 1. X-Ray Fluorescence.
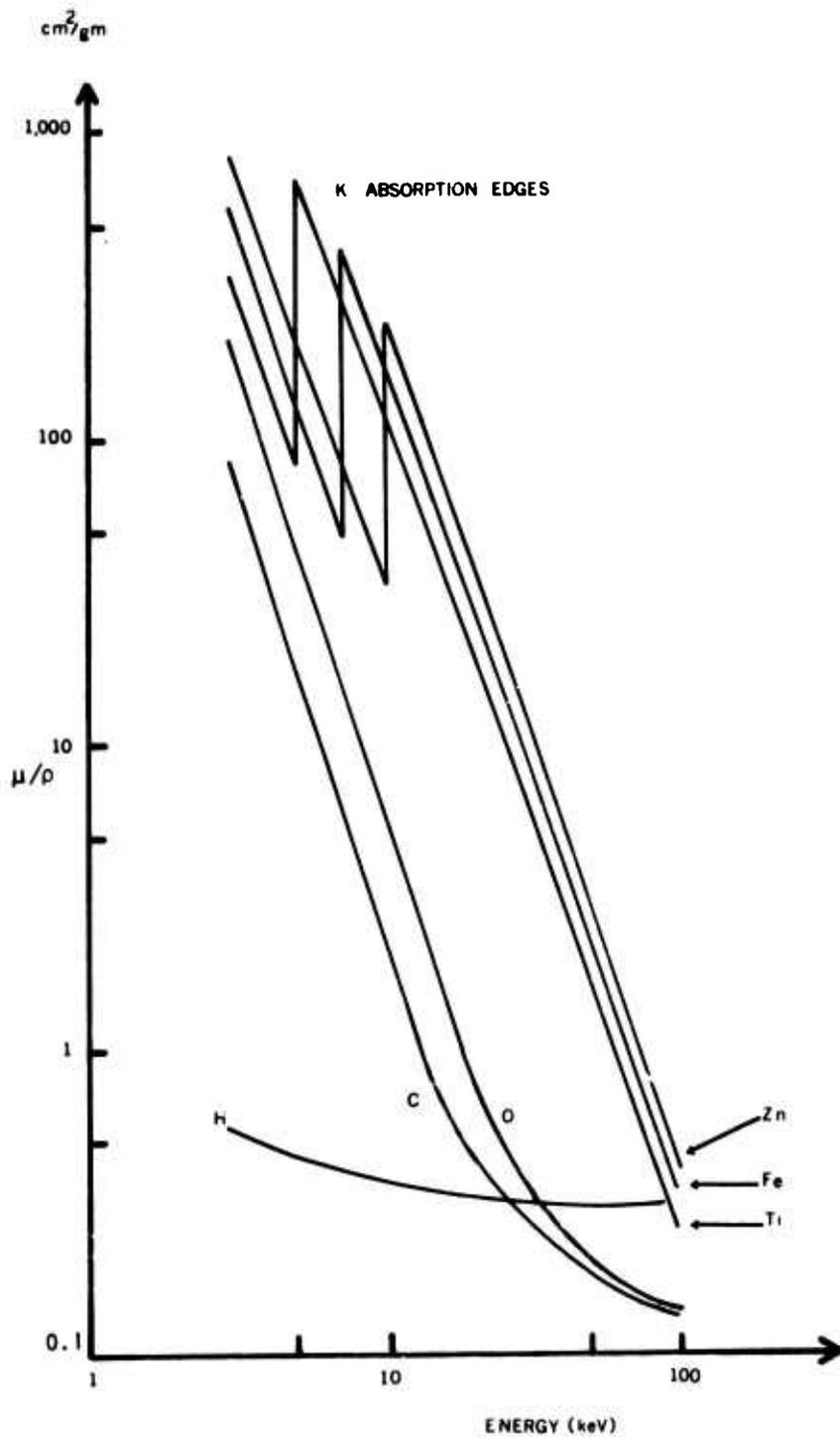
Figure 2. Mass Absorption Constant vs Energy.

5

TABLE I. X-RAY DATA				
Element	Atomic Number	Electron Binding Energy (kev)	X-Ray Fluorescence Yield	X-Ray Energy (kev)
Aluminum	13	1.560	≈0.03	1.487
Chromium	24	5.989	0.229	5.414
Iron	26	7.114	0.293	6.403
Copper	29	8.979	0.393	8.047

As shown in Figure 2, the probability for photon absorption is dependent upon the excitation source energy. The optimum source energy for XRF is one slightly greater than the K-shell binding energy. From Table I, we see that a source photon energy greater than 9 kev will fluoresce all the metals listed in that table.

A simple representation of how the XRF technique is applied in the ODM can be seen in Figure 3. In this illustration, the excitation source emissions stimulate XRF in the contaminated lubricant. Subsequently, the fluorescent X-ray emissions are sensed by the radiation detector. The detector's output is electronically conditioned to provide a readout which is proportional to contamination levels.

The emission of radiation is a statistical process, and the laws of statistics are applicable to all measurements based on radiation. The standard deviation (σ) defines a range of possible measured values within which the true value is contained with a certain probability (level of confidence). The standard deviation for a simple count measurement is given by the square root of the number of detected pulses:
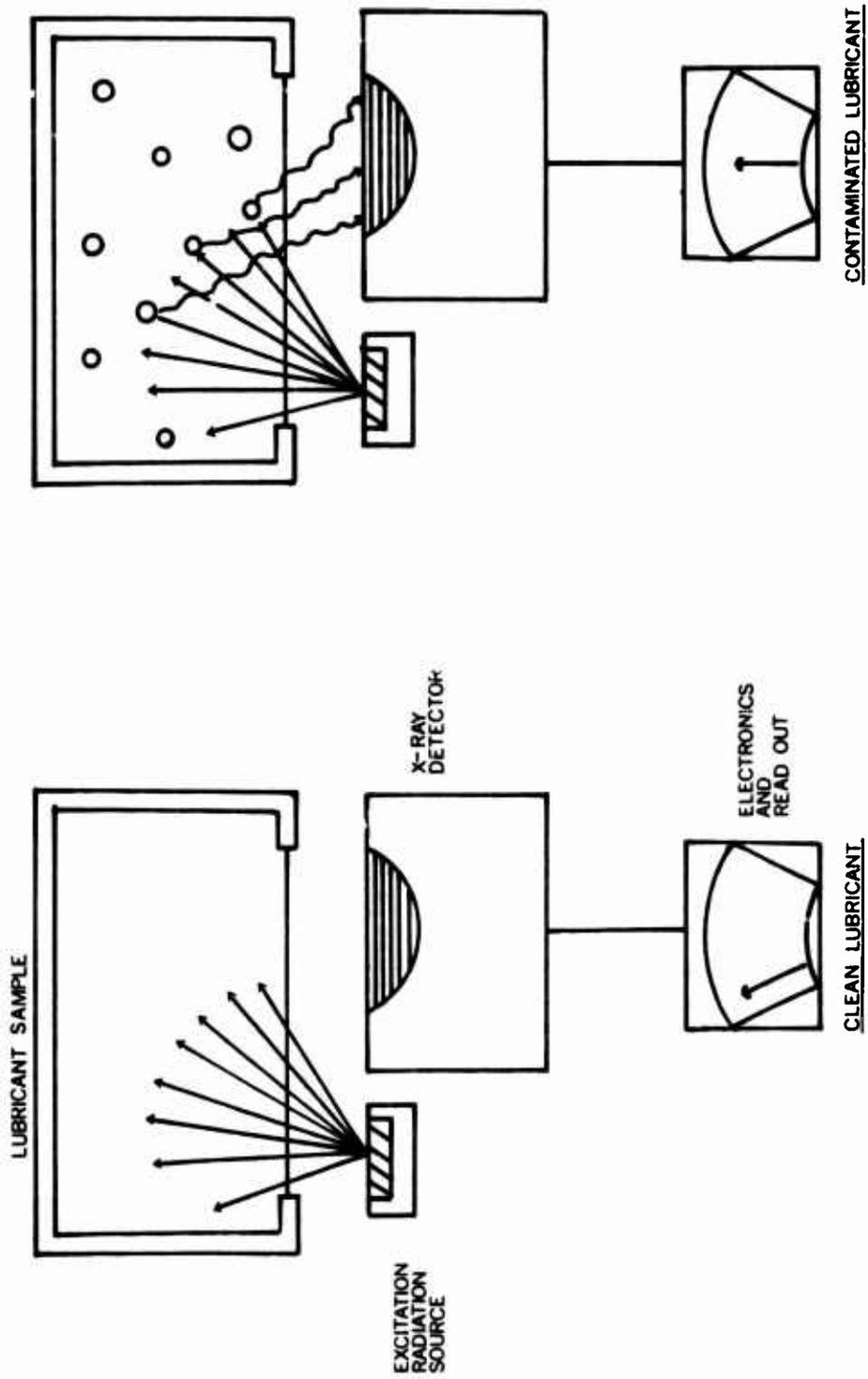
Figure 3. X-Ray Fluorescence in ODM.

CONTAMINATED LUBRICANT

X-RAY DETECTOR

ELECTRONICS AND READ OUT

CLEAN LUBRICANT

LUBRICANT SAMPLE

EXCITATION RADIATION SOURCE

STANDARD DEVIATION

Counts	$\sqrt{Counts}$	%
1	1	100
10	3.2	32
100	10	10
1,000	32	3.2
10,000	100	1

The significance of the standard deviation is best understood in connection with the confidence level. The probability is greater for the true value to be within the measured value's range of statistical uncertainty as one increases the confidence level of the certainty limits.

Number of σ	Confidence Level %
1	68
2	95
3	99

For example: The measurement of 10,000 counts results in a σ of 100 counts or 1%. Together with the confidence level, that means that with a probability of 68%, the result is 10,000 ± 100, i.e., within the range from 9,900 to 10,100. There is still a 32% chance that the actual value is either smaller than 9,900 or larger than 10,100 counts. However, if one takes an uncertainty range of three σ, then the true result will be, with a probability of 99%, within the range of 10,000 ± 300 or from 9,700 to 10,300, and only a 1% chance remains that the true value will be beyond these limits.

The same is true for all statistical accuracy statements. If an accuracy of 5% (3σ) is given for an XRF measurement, this means that with 99% probability, the actual value will be within a 5% range around the measured result. In other words, if one repeats the same measurement 100 times, 99 measurements will

give results which are all within ±5%; however, one measurement may give a result which is outside this range.

Count statistics associated with the Model 003 differ from the typical nuclear gauging application. The basic difference lies in the relative intensity of detected events, i.e., counts from the contaminant with respect to the background counts. The ODM is expected to operate under conditions where there are few contaminant counts (S) compared to B background counts. During ODM calibration, the value of B is determined precisely by taking count accumulations for long time periods. As a result, the mean measured value of B is essentially equal to the true value of B. This value is then entered into the instrument as a constant which is subtracted from the total count accumulation (C). Thus,

$$S = C - B \qquad\qquad (1)$$

The uncertainty in S (ΔS) is equal to the uncertainty in C (ΔC), neglecting the small uncertainty in the determination of B. Therefore,

$$\Delta S \approx \Delta C = \sqrt{C} \qquad\qquad (2)$$

and
$$\sigma s = \sqrt{C}$$

Background count rate is the dominant factor in defining the lower limit of contaminant detectability in the ODM.

3.0 COMPONENT/DESIGN STUDIES

The basic ODM consists of two parts: the contamination sensor head and the contaminant measuring electronics.

Operation of the system can be understood with reference to the block diagram, Figure 4. In the sensor head, radiation impinges on the sample, producing fluorescent radiation and background scattered radiation. This radiation is sensed in the radiation detector, producing charge pulses which are converted into analog voltage pulses in the amplifier module. The amplifier outputs voltage pulses where amplitude is proportional to the energy of the observed radiation.

Voltage discriminators are set to select pulses of desired amplitudes. The discriminators generate a standard logic pulse each time the system detects an X-ray from the element being studied (i.e., iron). During the sampling period the gate is open and the logic pulses are counted in the data accumulator. At the end of the sampling period the number of counts is strobed into the data converter. By choosing the correct type of data conversion, the amount of contaminant element can be outputted in terms of parts per million, absolute mass of contaminant, or other engineering units.

The simplicity of operation and stability of the contaminant monitor are due to the Automatic Gain Control (AGC) system. This system is also shown on the block diagram (Figure 4). Radiation from a small calibration source is emitted directly into the detector. The AGC system monitors the amplitude and number of pulses from this source and adjusts the detector high voltage to maintain constant system gain. This feedback loop operates continuously; it removes the requirement for frequent recalibration and gain adjustments. Many common nuclear gauging system defects, such as aging of components, count rate sensitivity, or gain changes in amplifier circuits, are automatically nullified by the AGC system.

The choice of radiation source and source-detector geometry must be carefully designed to insure maximum sensitivity. The source must be chosen to maximize X-ray production for those elements of interest and have desirable radiation safety properties as well. The source-detector geometry must be designed to minimize radiation scattering. The structural materials of the sensor head - particularly around the source, sample, and detection area - should be free of the element being detected. The other key factor in the source-detector geometry is the detector itself. The physical configuration of the detector, fill gas composition and pressure, and detector window area have significant bearing on the ultimate performance of the ODM.
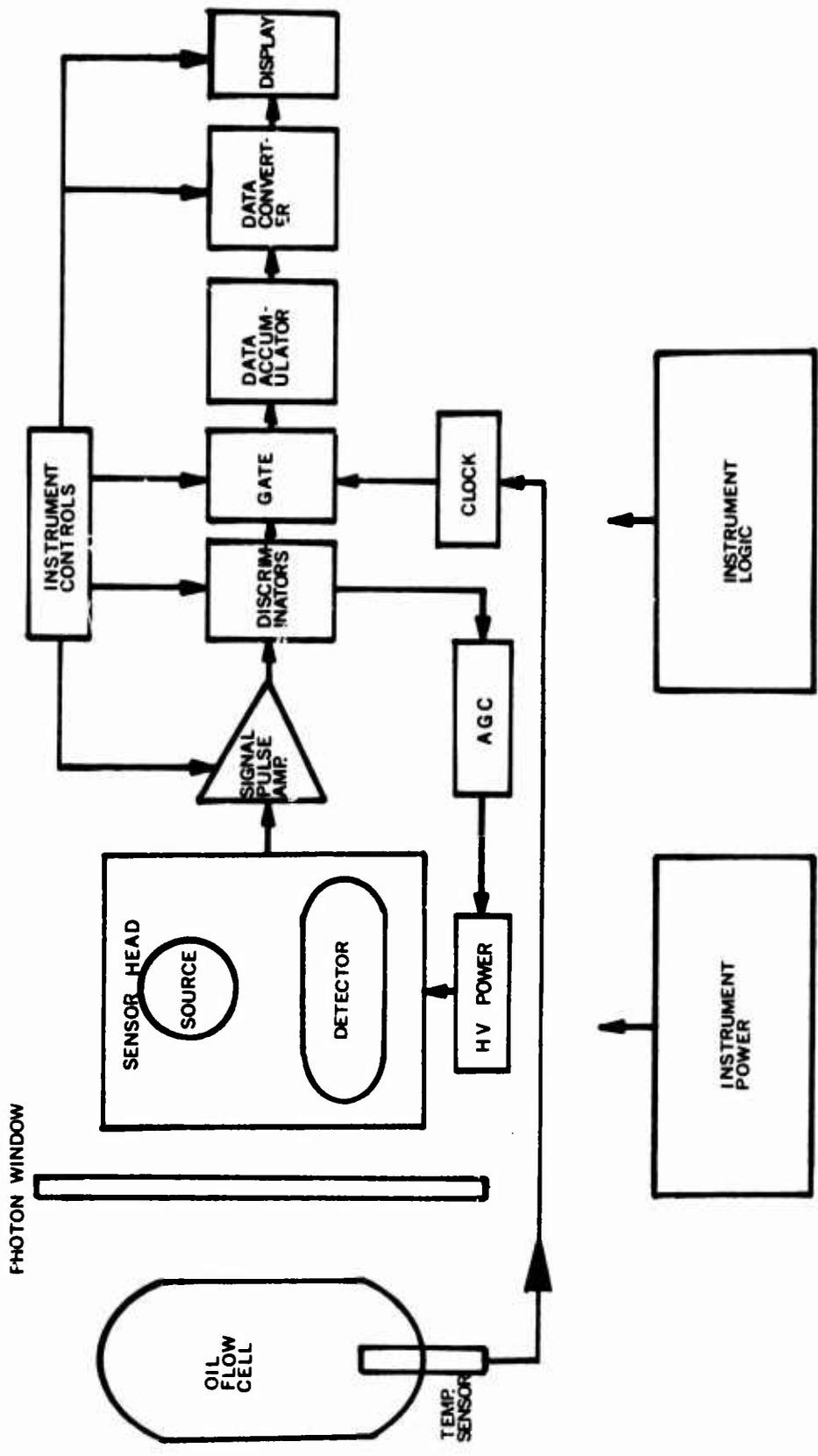
Figure 4. ODM Block Diagram.

11

Since the ODM is intended for in-line measurements, it is necessary to provide an appropriate flow-cell (i.e., one which obtains representative oil samples). It must provide positive oil containment while allowing XRF measurements to take place. Hence, a photon "window" is required which can withstand oil pressure and temperature stresses with minimal photon attenuation.

The oil temperature can range from $100^{\circ}F$ to $300^{\circ}F$. The density will change from 0.929 to 0.891 gram per cubic centimeter during that temperature change in MIL-L-7808 oil. Thus, there are changes in radiation scatter and attenuation characteristics brought about by this density change. The radiation detector also exhibits changes in both gain and resolution over the temperature range of interest. To assure that the aforementioned temperature effects are minimized, electronic countermeasures are employed.

Each of the component and design factors just presented in brief form were generally defined during the previous feasibility study[1]. The efforts in specific definition for the ODM are detailed in the remainder of this chapter.

3.1 RADIATION SOURCE

There are two general source types appropriate for use in XRF: primary and secondary photon sources. The former are those radioactive nuclides which emit photons in the energy range of interest. The latter are sources producing photons by charged particle interactions in a target material. These photon generators employ a radioactive nuclide which emits energetic charged particles in its decay process. In the case of a secondary photon source, the photon energy produced is determined by the target material.

3.1.1 Krypton-85 Source Design

Effort was directed toward development of an X-ray excitation source which employed Krypton-85 betas and a molybdenum target. These secondary photon sources contain 120 millicuries of Krypton-85.

The use of a radioactive nuclide of a noble gas is highly desirable from the standpoint of radiological safety, particularly with a gauging technique having potential use in an airborne application. Krypton-85 has a half-life of 10.76 years; its principal decay mode is beta emission (0.67 Mev max.). Photons of 0.514 Mev are also emitted with an abundance of 0.41%.

12

The process of interest for source photon production is beta-induced ionization in the K-shell of target atoms with subsequent emission of K X-rays. The characteristic X-rays produced with the molybdenum target are 17.44 and 19.65 Kev for the Kα and Kβ X-rays, respectively. Relative abundances are 84% (Kα) and 16% (Kβ). In molybdenum, the decimal fraction of K-shell vacancies which give rise to K X-rays is 0.73.

Another interaction process is beta particle deacceleration; this phenomenon produces bremsstrahlung radiation. Bremsstrahlung production is extremely undesirable for this application because of its substantial contribution to the background.

The attenuation of beta particles through an absorbing medium can be expressed by the equation

$$I = I_o e^{-(\mu/\rho)\rho x} \tag{4}$$

where   I = beta flux through material thickness of x

   x = material thickness, cm

   I_o = beta flux at x = 0

   μ/ρ = mass absorption coefficient attenuating
          material (cm^2/gm)

   ρ = material density (gm/cm^3)

As presented by Evans[5], the mass absorption coefficient is a function of the maximum beta energy (E_m) and the absorber's atomic number (Z) and atomic weight (A_w):

$$\mu/\rho = \frac{35Z}{E_m^{1.14} A_w} \qquad \text{for } Z \leq 13 \tag{5}$$

and $$\mu/o = \frac{17}{E_m^{1.14}} \qquad \text{for } Z \geq 13 \tag{6}$$

13

In molybdenum, Kr-85 betas have a linear absorption coefficient of 1.44 per centimeter. However, self-absorption of the Mo X-rays in the target material establishes the upper limit in effective material thickness. The linear absorption coefficient of Mo K X-rays in molybdenum is 188 per centimeter. Thus, there is a tradeoff between the target thickness needed for reasonable beta-target interactions and the resultant X-ray self-absorption. The number and energy of bremsstrahlung photons are proportional to both E_m and Z. Therefore, target thickness is also a determinant factor in bremsstrahlung production. Thickness should be kept to a minimum to reduce this effect.

The first source package design which was evaluated is illustrated in Figure 5. The gas cavity was lined with molybdenum to enhance Mo X-ray production. Both the liner and window were 0.127 mm thick (0.13 g/cm^2). Since this target thickness permitted transmission of about 45% of the initial beta flux, a 0.75 mm thickness of beryllium was placed over the Mo window to absorb these betas.

After evaluation of the first configuration, a second was designed and fabricated. This source design is illustrated in Figure 6. Significant design changes included reduction of source package diameter, addition of an inner liner of beryllium, a beryllium filter, and an aluminum housing. The changes produced a reduction in bremsstrahlung and improvements in source-detector geometry. The Kr-85/Mo source testing is detailed in the following subsection.

3.1.2 Kr-85/Mo Source Tests

Numerous tests were performed with the gas-filled, molybdenum X-ray sources to evaluate their radiation characteristics and obtain maximum performance for oil contaminant excitation. Figures 7 and 8 present the effect on detected energy distribution as a function of beryllium beta-absorber thickness. These studies show a 0.75 mm thickness of beryllium to be optimum. The background count rate in the energy region of the Fe X-rays was still unacceptably high; a substantial portion of this was attributed to the bremsstrahlung production in the molybdenum liner. Figure 9 shows the radiative yields (i.e., bremsstrahlung production) of molybdenum, aluminum, and beryllium as a function of beta energy. The effect of the change in liner material (replacing the Mo liner with a Be liner) is shown in Figure 10. Unfortunately, the Mo target also produces bremsstrahlung in addition to the Mo X-rays. Hence, the bremsstrahlung cannot be totally eliminated.

14

WINDOW: .005 Mo
FUSION WELDED

$\frac{15}{16}$ DIA

$1\frac{3}{16}$ DIA

$\frac{7}{8}$ DIA

ACTIVITY CAVITY: APPROX.
VOLUME OF 5cc
LINED W/.005 Mo

FUSION WELDED

$\frac{1}{8}$ HOLE—(4) PLCS ON 90° SPACING

$1\frac{3}{32}$

$\frac{3}{32}$

$1\frac{5}{8}$ HC.

$1\frac{15}{16}$ DIA

LOAD SEC: $\frac{1}{8}$ OD Cu TUBING, SEALED
BY COLD WELD

MAT'L: 304L STN STL.
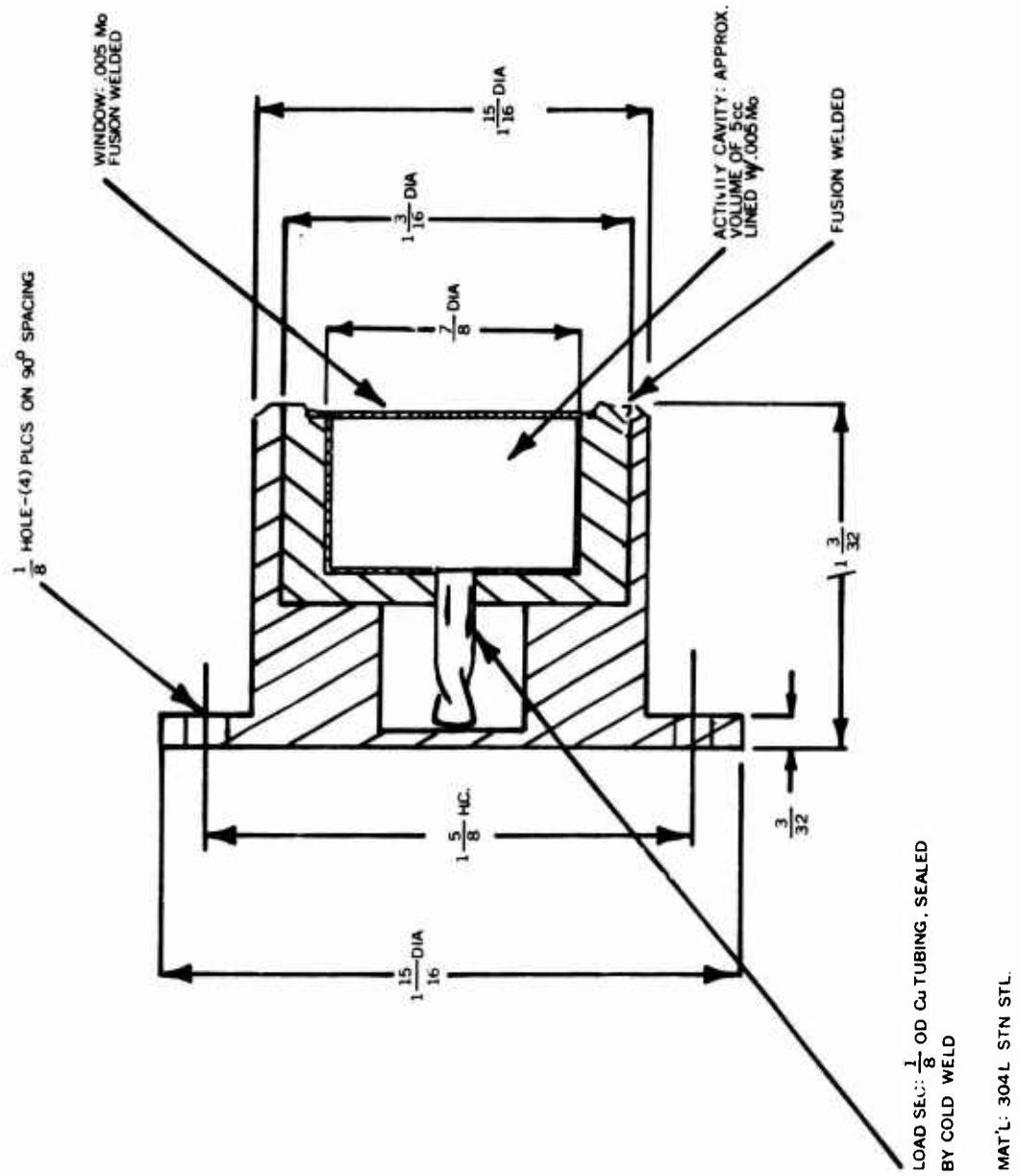
Figure 5. Kr-85 Beta Capsule Design.

WINDOW : 0.005" THK MOLYB-
DENUM (BRAZED)

FILTER : 0.030" THK
BERYLLIUM

1 DIA

55/64 DIA

19/32 DIA

ACTIVITY CAVITY : APPROX.
VOLUME OF 2cc

LINER : BERYLLIUM

HOUSING : 1100 ALUM- NOT
INTEGRAL TO CAPSULE

FUSION WELD

$1\frac{7}{32}$

$\frac{1}{8}$

$\frac{3}{32}$ HOLE.(4) PLCS

LOAD SEC : $\frac{1}{8}$ Cu TUBING, SEALED BY COLD WELD

CAPSULE : 304 STN STL

$1\frac{5}{32}$ H.C.

$1\frac{1}{2}$ DIA
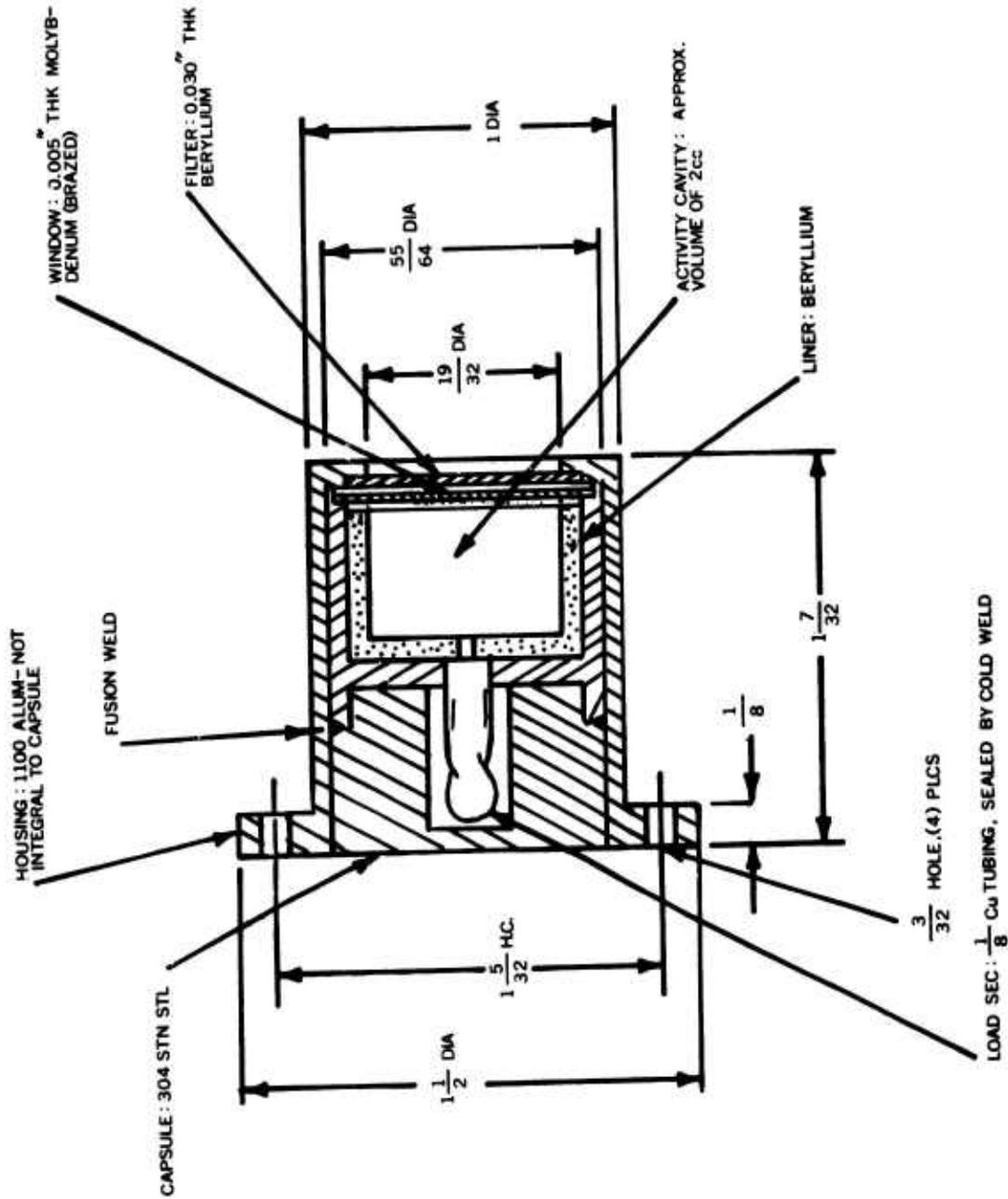
Figure 6. Kr-85/Mo Capsule Design.

16
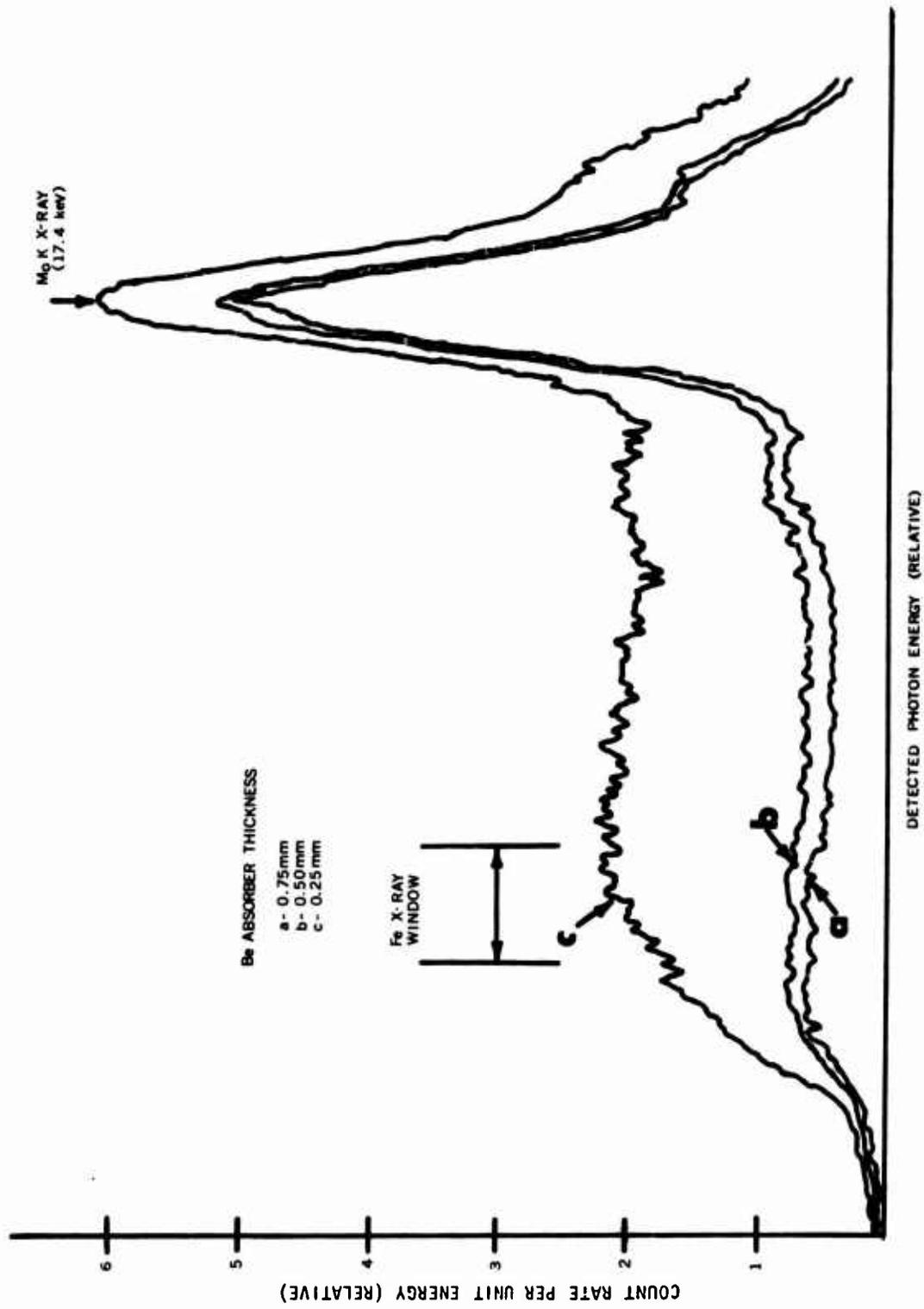
Figure 7. Photon Energy Distribution vs Filter Thickness.
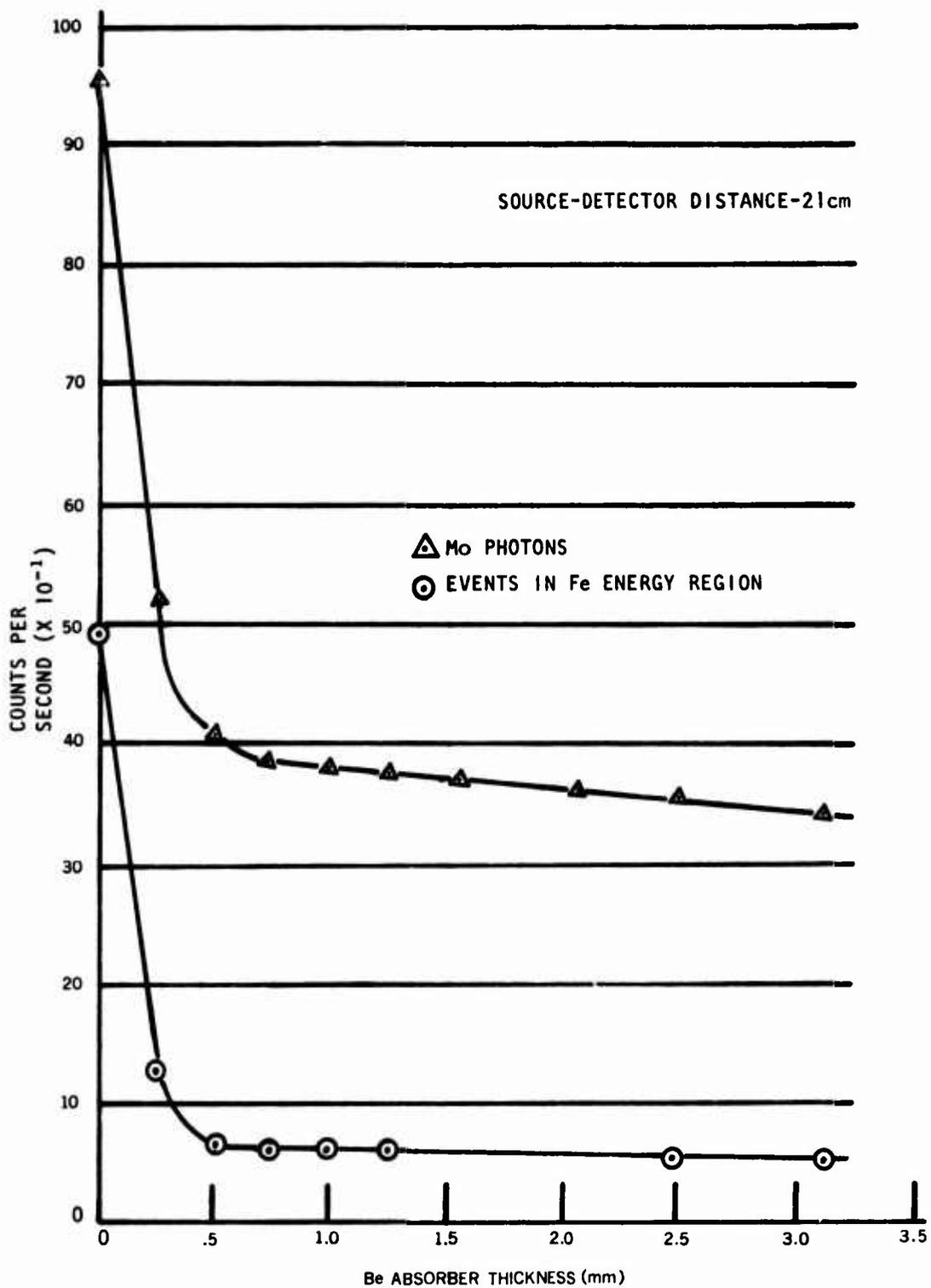
Figure 8. Photon Intensity vs Filter Thickness.
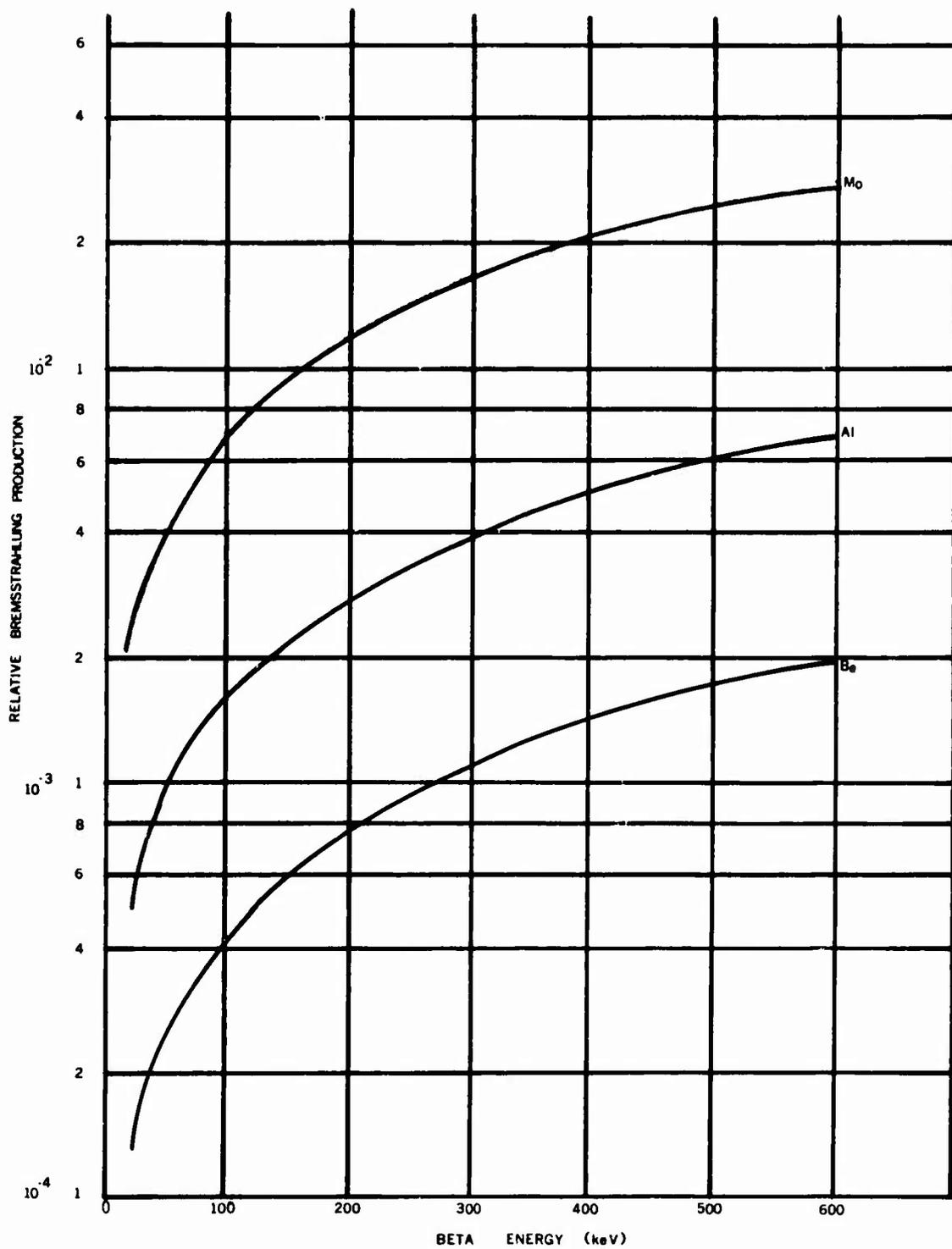
Figure 9. Radiative Yields.

19
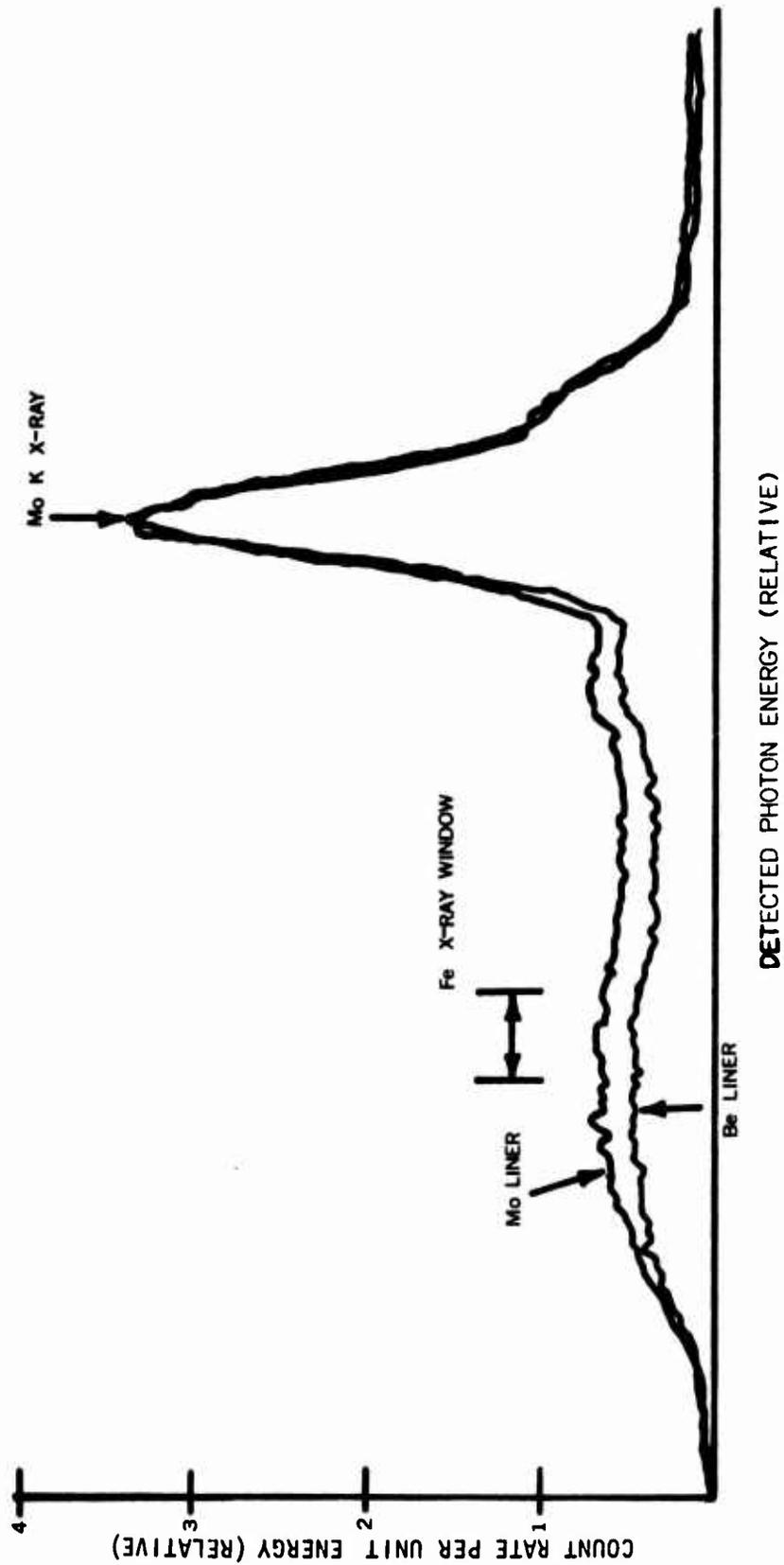
Figure 10. Comparative Spectral Distributions - Mo vs Be Liner.

The major remaining source contribution to the count-rate in the iron X-ray energy region was determined to be Compton interactions from the Kr-85 decay gammas (0.514 Mev). Figure 11 shows the detected energy distribution from a Kr-85/Mo source through the detector window and through the side of the detector (its wall material is 0.8 mm steel with an inner liner of 0.5 mm aluminum). The count-rate in the iron energy region from photons passing through the detector wall is approximately 60% relative to that passing through the detector window. Lead shielding fails to adequately reduce the rate of Compton interactions from the energetic photons through the source and detector walls. The linear attenuation coefficient for 0.5 Mev gammas in lead is 1.79 per centimeter. Hence, one cannot achieve sufficient shielding while maintaining a satisfactory source-oil sample-detector geometry.

The discussions regarding the Kr-85/Mo sources have stressed the need for "spectral purity" whereby a minimum number of detected photon events occur in the region of the Fe X-rays. Only by keeping this detected event rate to a very low level can one achieve adequate measurement sensitivity.

The detected photon energy distribution is substantially degraded in quality when the source-detector geometry is set up in the ODM configuration. Two factors contribute to the spectral degradation: (1) the close proximity of the Kr-85/Mo source to the detector (necessary for effective XRF production and detection), and (2) photon energy degradation and scatter in the oil and oil containment hardware.

Figure 12 is a graphic presentation of these effects. The background count rate increases by almost a factor of 2 as the oil and flow-cell hardware are positioned over the source-detector assembly. With the flow-cell cover removed, 15-micron-diameter iron particles were added to the oil. A mass of 7.9 mg was detectable, but a mass of 1.8 mg was not. Figure 13 presents detected photon energy spectra from those measurements. The poor "signal-to-noise" ratio (i.e., ratio of iron XRF plus background-to-background alone) dictated the need for substantial additional effort in the area of source development. Since this was not permitted within the program's schedule and funding, the decision was made to use a different radioactive material as the excitation source.

3.1.3 Plutonium-238 Source Tests

Significant effort was directed to the consideration of various excitation sources during the previous program[1]. Of those considered, Plutonium-238 (Pu-238) was judged to be the most appropriate and was subsequently used to demonstrate concept
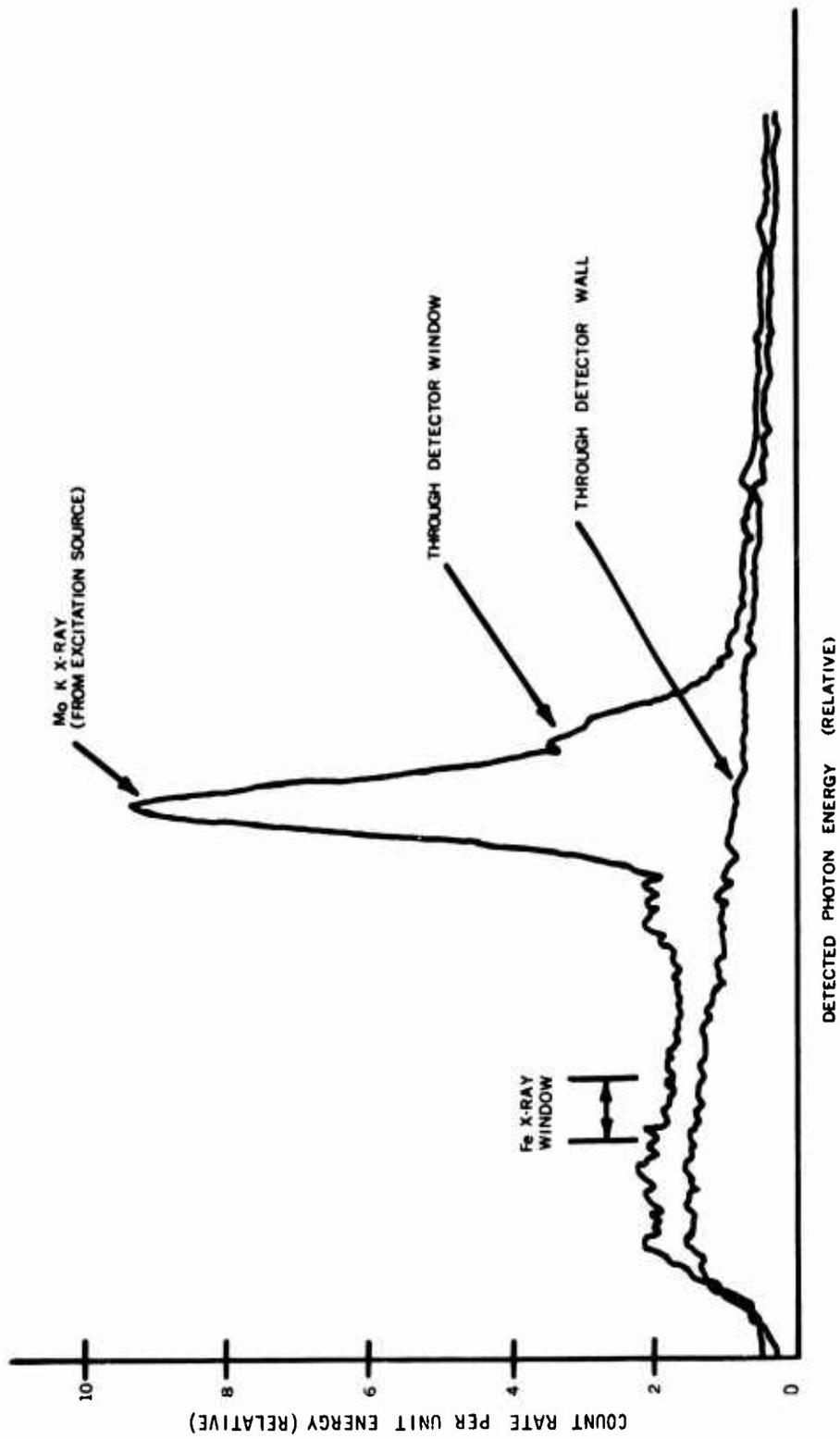
Figure 11. Compton Events in Detector.

22
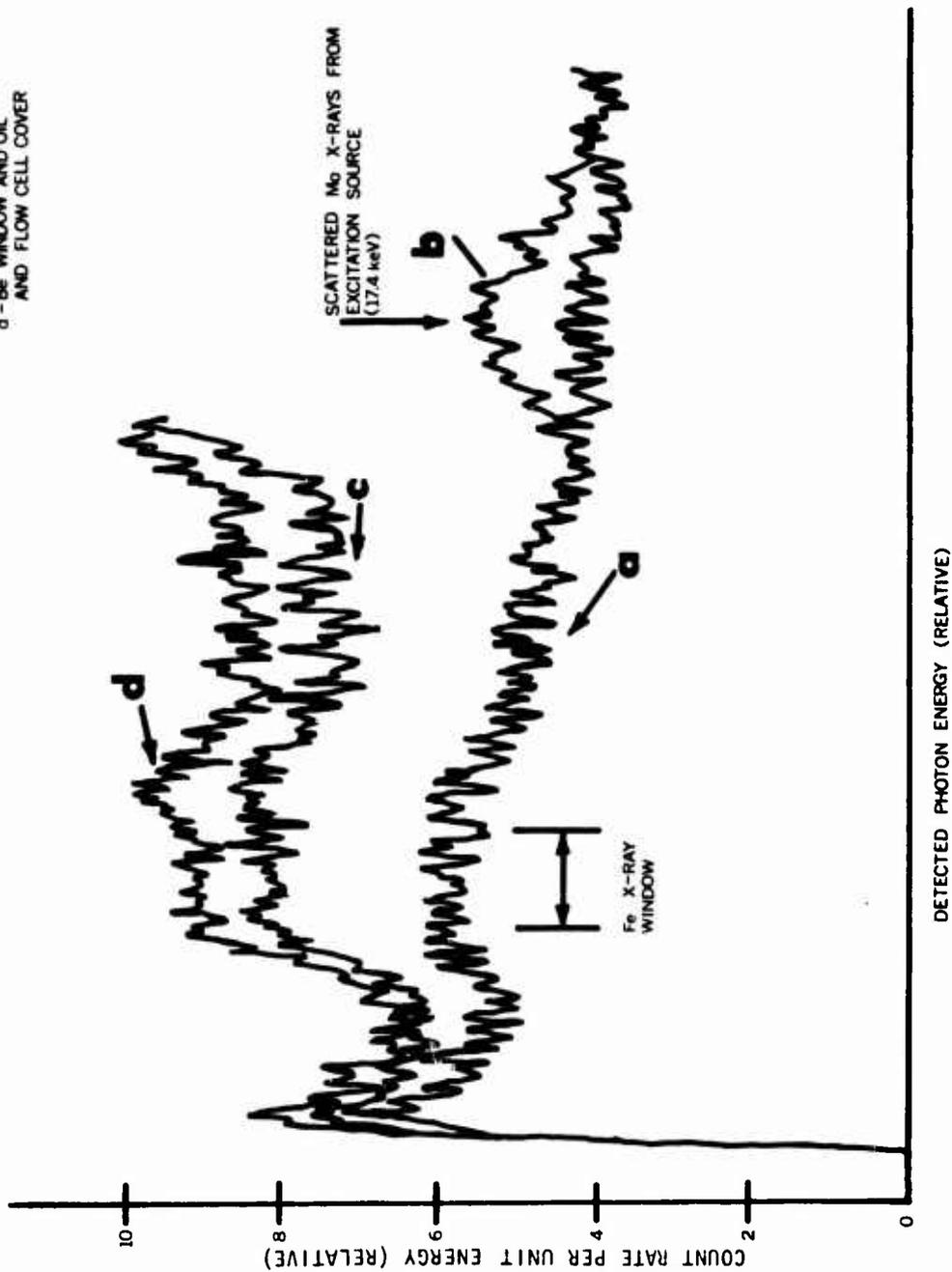
Figure 12. Background Buildup From Flow-Cell Masses.

23
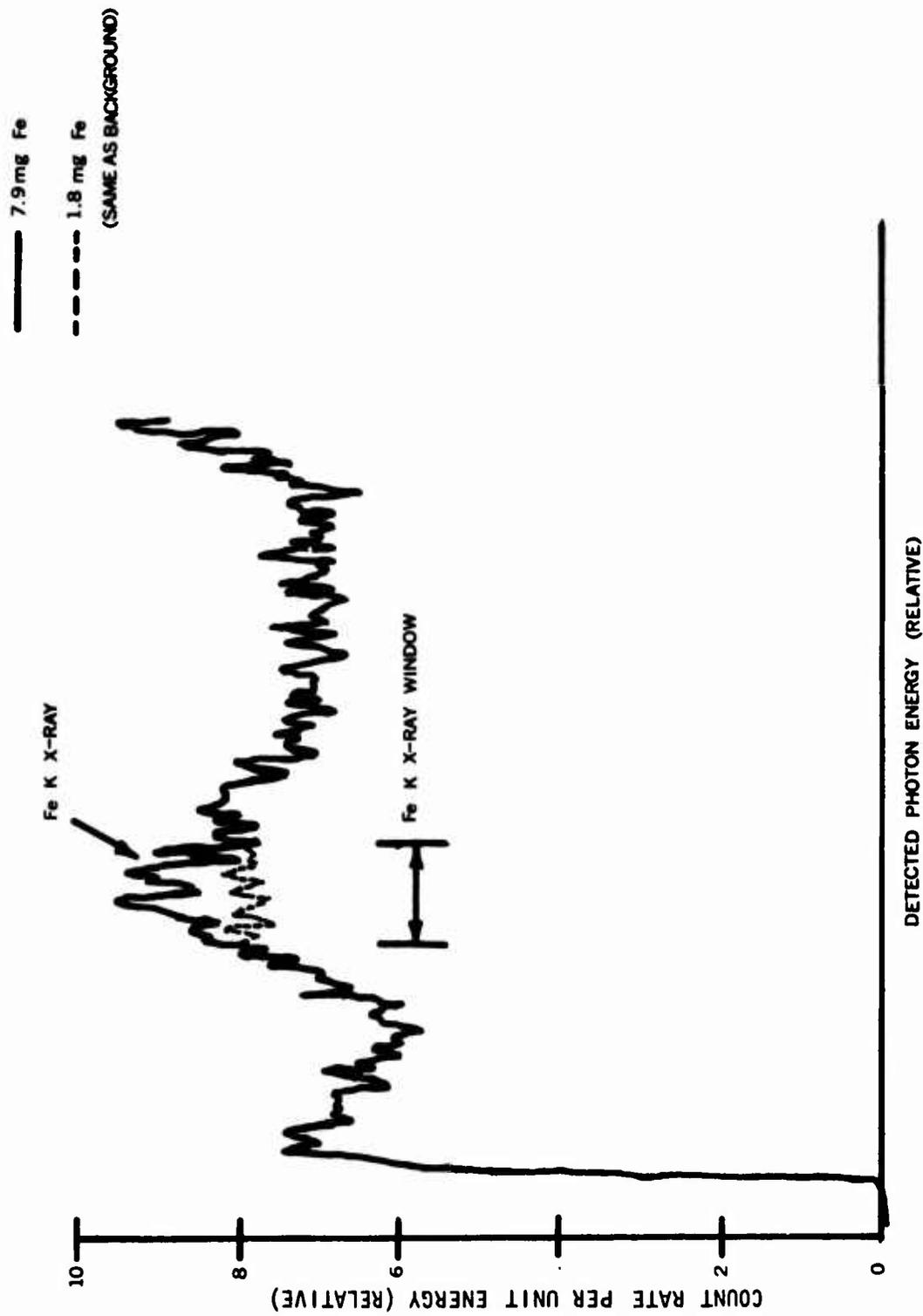
Figure 13. Detected Iron Spectral Distribution.

24

feasibility. For similar reasons, this radioactive material was selected for use in the ODM to overcome the disadvantages of the Kr-85/Mo source.

Plutonium-238 has an 86-year half-life; it decays by alpha particle emission to uranium-234. Approximately 13% of the decays also produce uranium L X-rays. The major X-ray photons are at 17.7 and 13.9 Kev, with the latter being emitted at 0.7 times the rate of the former. Source strengths of 10 and 30 millicuries were used in the first and second ODMs, respectively.

The capsule which holds the plutonium is constructed to contain the radioactive material and its alpha emissions, thus allowing only the X-rays to escape. Inside the source capsule, a tungsten alloy shield is placed around the sides and back of the radioactive disc so that the X-ray photons have a spatial distribution which is slightly less than 2π steradians.

There are disadvantages associated with the use of a Pu-238 source in the ODM. Its biological half-life is long with respect to that of Kr-85 (i.e., 200 years compared to less than 0.01 year for Kr-85). The physiochemical nature of plutonium causes it to have a biological toxicity far greater than that of the krypton radioisotope. Its use is therefore generally limited to ground-based applications by personnel having a specific radioactive material license to possess and use it. One additional disadvantage exists with the specific Pu-238 source capsules used in the ODM. The tungsten alloy shield is fluoresced by the source; this produces a noticeable increase in the background level. The predominant tungsten L X-ray is at 8.4 Kev.

Figure 14 presents comparative detected energy spectra from Kr-85/Mo and Pu-238 sources. The advantages offered by the plutonium source are clearly evident in Figure 14(b). The count rate in the iron energy region is one-tenth that of the Kr-85/Mo source. The average photon energy of Pu-238 is lower since it also emits 13.9 Kev X-rays. The Pu-238 photon emission rate is approximately 130 times greater than that of Kr-85/Mo for the same source decay rate; hence, the probability for XRF production is enhanced by a factor of 170 for a given source activity level.

The relatively small size of the plutonium source compared to the gaseous Kr-85 source allows for a closer source-oil sample-detector geometry and results in improved efficiency for detecting the metallic contaminant. Comparative measurements with ODM hardware showed that Pu-238 gave 2000 times greater sensitivity than Kr-85/Mo.
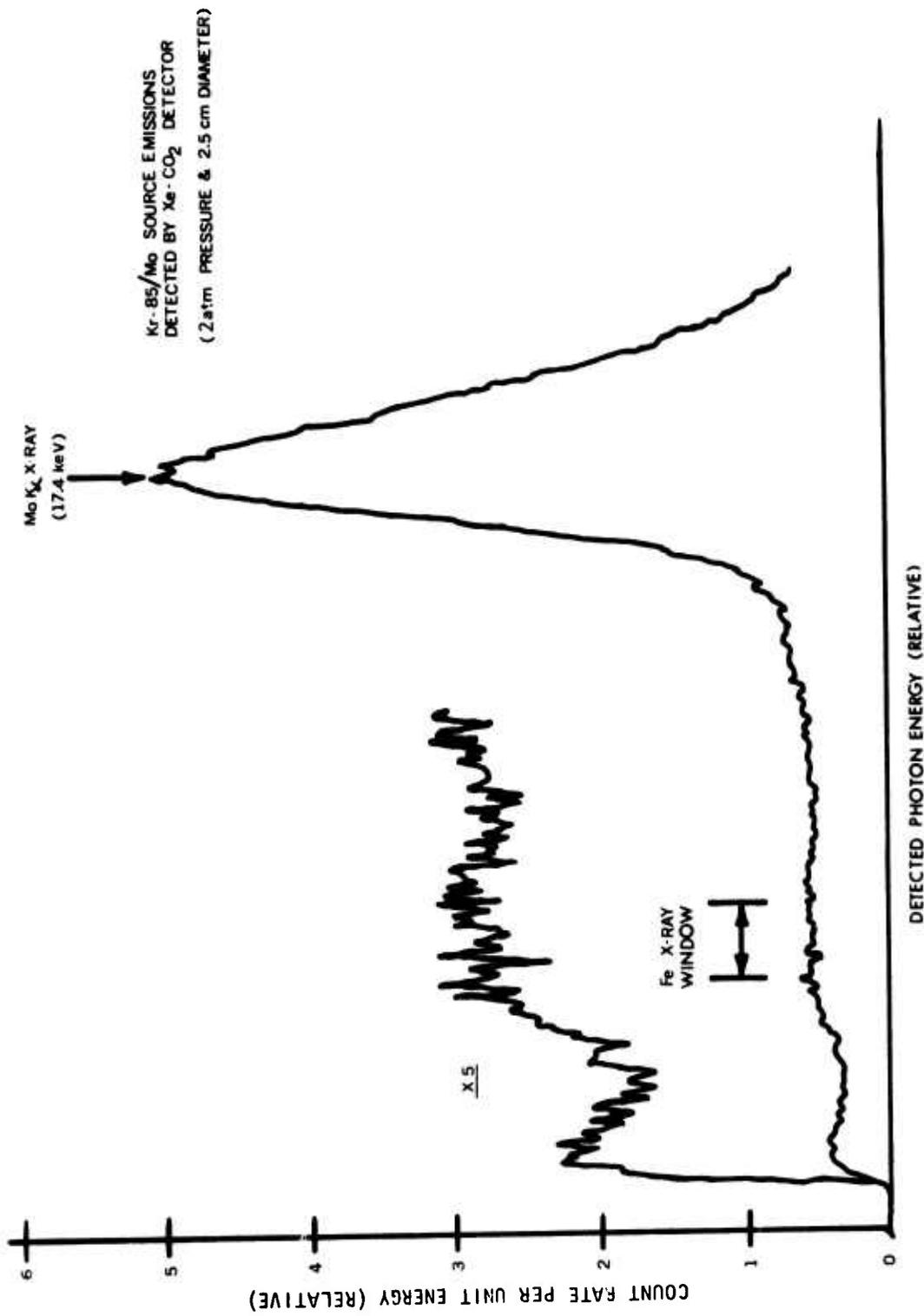
Figure 14(a). Spectrum From Kr-85/Mo.

Figure 14(b). Spectrum From Pu-238.

Pu-238 SOURCE EMISSIONS
DETECTED BY Xe-CO$_2$ DETECTOR
(2atm PRESSURE AND 2.5cm DIAMETER)

U L$_\beta$ X-RAY
(17.7keV)

U L$_\alpha$ X-RAY
(13.9keV)

Fe X-RAY WINDOW

X5

COUNT RATE PER UNIT ENERGY (RELATIVE)

DETECTED PHOTON ENERGY (RELATIVE)

27

Due to the radioactive decay characteristics of this radio-species, its source emissions are easily shielded. Thus, essentially all radiation is confined within the ODM sensor head. The radiation level at the external surface of the probe is less than 0.2 milliroentgen (mR) per hour. This level is well below the limit set by the United States Atomic Energy Commission - even with the assumption that the person is in close, continuous contact with the ODM sensor head.

3.2 RADIATION DETECTOR

The detector type used in the ODM systems is a proportional counter tube. Detectors of this type have the capability of X-ray energy discrimination and provide sufficient energy resolution for this application.

When a monoenergetic X-ray flux is sensed by the detector, its average output pulse amplitude is proportional to the detected photon energy. The pulse height distribution about that average defines the detector's ability to resolve adjacent photon peak energies. Pulse height distribution is expressed in units of energy - or energy percentage - for the full width at one-half the maximum pulse distribution height (FWHM).

Resolution is an important criterion in the performance of an X-ray detector. Within the energy region of interest (i.e., 1.5-8 Kev), proportional counter tubes provide energy resolution on the order of 0.9-1.4 Kev.

The laboratory test instrument detector[1] was a proportional counter tube 5 cm in diameter, 18 cm in length, and filled with 1 atmosphere of 97% argon and 3% of carbon dioxide. The overall size made it difficult to provide a sensor assembly which was compatible and easily interfaced with the UH-1 transmission and 90° gear box. To alleviate this condition, another tube 2.5 cm in diameter and 12 cm in length was selected for use with the ODM. Its detection area (2.84 cm^2) is 56% of that provided by the previous unit.

Detection efficiency is a direct function of detection area. To counteract a reduction in detection area, one can increase fill-gas pressure or change the gas composition. The detection efficiency is a function of detecting gas thickness. The interaction probability of a photon traversing an energy-absorbing gas medium can be expressed by

$$I/I_o = 1 - e^{-\mu x} \tag{7}$$

where I_o = initial photon flux, photons/cm²/sec

I = photons which interact, photons/cm²/sec

μ = linear absorption coefficient, cm²/g

x = absorber thick, g/cm²

The value of μ for argon and xenon is 225 and 560 cm²/g, respectively, for the 6.4 Kev Fe X-rays. With equation (7), the laborabory test unit's detection efficiency is calculated to be 91%. When one takes into account the reduction in detection area and tube diameter, an ODM detector with 1-atm Ar-CO_2 fill-gas would exhibit a relative detection efficiency of 56%. A relative detection efficiency of 62% would be provided by 1-atm Xe-CO_2 ODM detector. Thus, one can partially negate the reduction in detection efficiency caused by the smaller detection area.

Althouth one does not significantly increase the detection efficiency for Fe X-rays by going to 2 atm Xe-CO_2 fill-gas with a 2.5 cm diameter detector, there are other advantages to be gained. Such a unit offers an increased probability that more energetic photons will deposit a greater fraction of their energy in the sensitive gas volume. Hence, the net effect is a relative reduction of low-energy Compton events. This serves to reduce the relative detected background contribution in the energy region of the Fe X-rays. Figures 15 and 16 show the energy distributions from a Kr-85/Mo source as detected with a 5-cm dia., 1 atm Ar-CO_2 tube (Figure 15) and a 2.5-cm dia., 2 atm Xe-CO_2 tube (Figure 16). The relative reduction of detected Compton events is graphically evident by a comparison of these two spectra: it is approximately 10% less with the latter tube.

A minor background contribution can result from iron contamination in the detector's beryllium window and from indiscriminate use of the copper-based braze material used to mate the beryllium window with the detector body. Figure 17 shows the comparative energy distributions of fluorescent X-rays from three different Xe-CO_2 detector windows. The metal contamination in the Be window and adjacent braze material is even more graphically presented in Figure 18 as detected with an Ar-CO_2 detector with superior energy resolution.
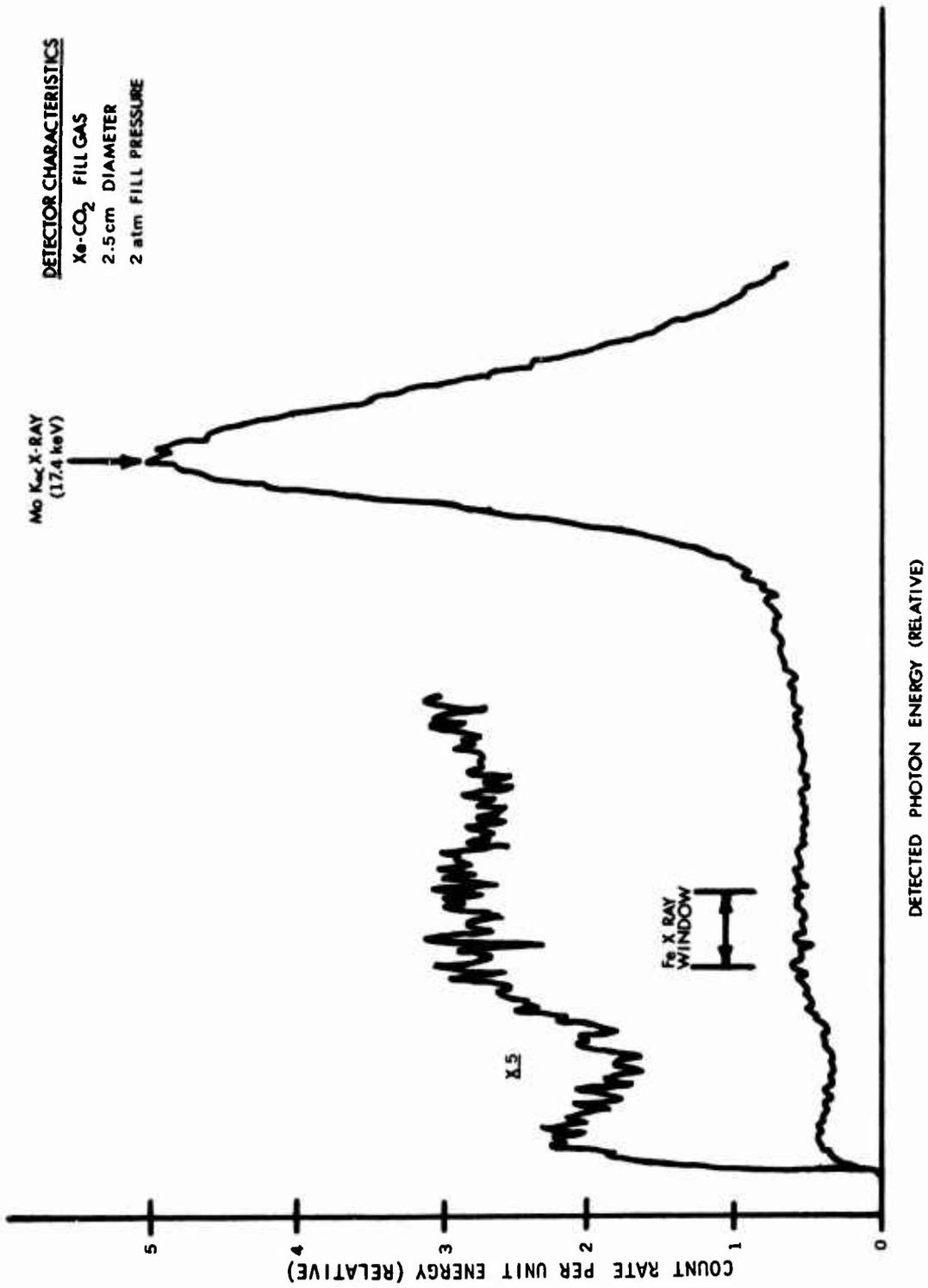
Figure 15. Detected Energy Distribution With Ar-CO$_2$ Tube.

DETECTED PHOTON ENERGY (RELATIVE)

COUNT RATE PER UNIT ENERGY (RELATIVE)

0 1 2 3 4 5

DETECTOR CHARACTERISTICS

Xe-CO$_2$ FILL GAS
2.5 cm DIAMETER
2 atm FILL PRESSURE

Mo K$_\alpha$ X-RAY
(17.4 keV)

Fe X RAY
WINDOW

X5
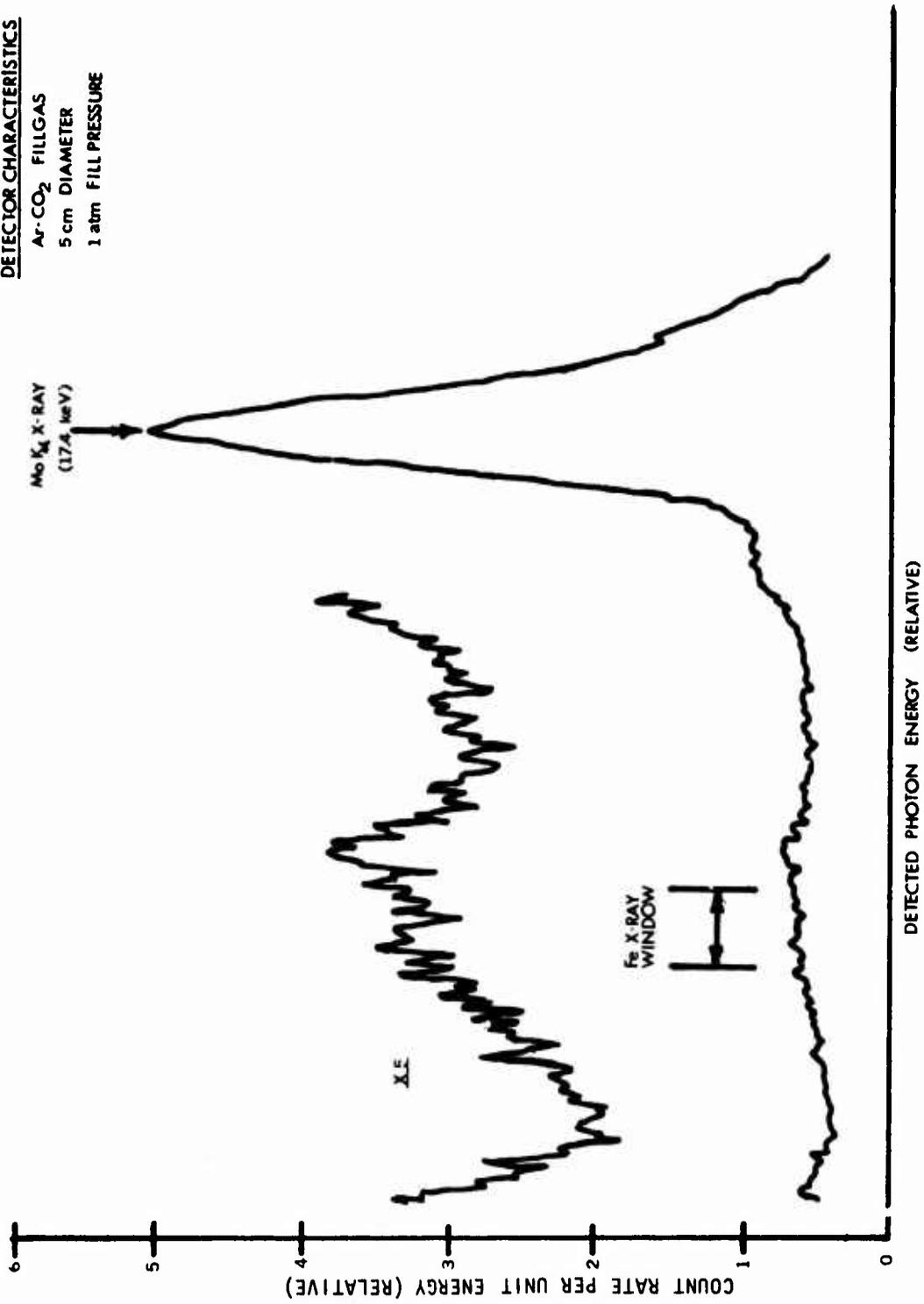
Figure 16. Detected Energy Distribution With Xe-CO$_2$ Tube.

DETECTOR ✳ 2837

DETECTOR ✳ 2844

DETECTOR ✳ 2845

Cu K X-RAY (8.0 keV)

SCATTERED W X-RAY (8.4 keV)

Fe K X-RAY (6.4 keV)

Fe X-RAY WINDOW

DETECTED PHOTON ENERGY (RELATIVE)

4 K OFFSET

2 K OFFSET

2

1

0

1

0

1

0

COUNT RATE PER UNIT ENERGY (RELATIVE)
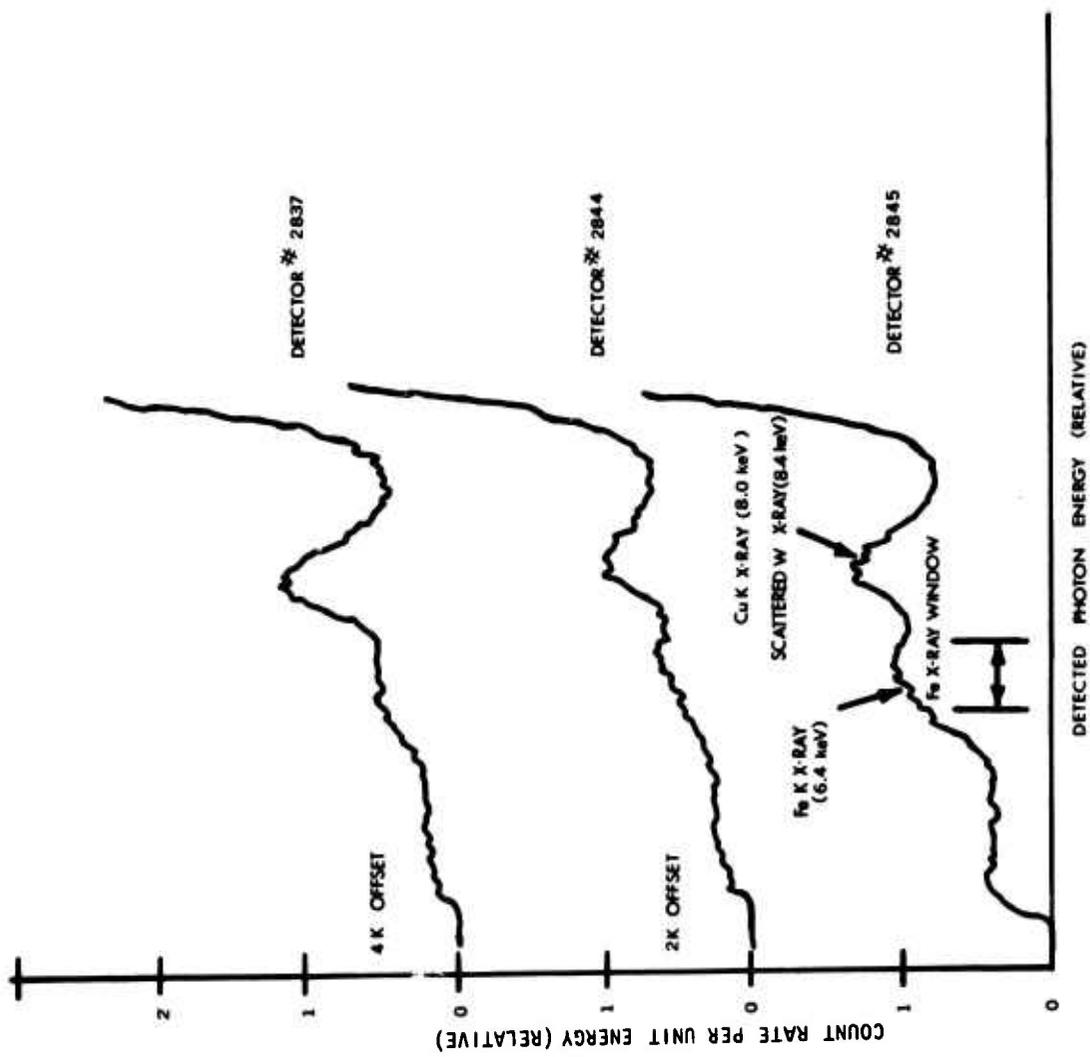
Figure 17. Detector Window Contamination.

The comparative spectral distributions in Figures 17 and 18 are also a very graphic demonstration of the importance of detector resolution in the evaluation and identification of low contaminant concentrations.

3.3 BERYLLIUM WINDOW

As discussed in Section 3.0, a thin metal plate separates the radiation source and detector hardware from the lubricant sample volume. This "window" must exhibit: (a) minimum attenuation to source and sample photons, (b) thermal and chemical compatibility with the oil and (c) sufficient strength to withstand a probable pressure differential between radiation hardware and oil. The material which best satisfies these criteria is beryllium.

A 10-mil Be thickness attenuates less than 2% of the excitation source photons and less than 10% of the iron K X-rays. The same thickness of aluminum would attenuate more than 99% of the iron X-rays. Although organic materials can provide a photon transparency like that of beryllium, they cannot satisfy the other criteria.

The task of incorporating a thin Be window in the aluminum flow-cell was not easily accomplished. It was initially planned that the units would be electron-beam welded. The use of electron-beam welding was unsuccessful in this case. Thermally-induced stresses caused windows to fracture during the weld operation. The linear coefficient of thermal expansion for aluminum is over a factor of two greater than that of beryllium (12.5 and 6 in./in.^{0}F x 10^6 for Al and Be, respectively). A successful weld can be achieved by taking both metal members to a temperature within 20^0F (nominal) of the aluminum's melting point with a subsequent slow cool-down to allow for stress relief. The facility doing the weld operation was unable to provide sufficient control of the local thermal environment.

Subsequent to weld difficulties (and the total loss of Be window stock because of the fractures), another subcontractor provided both additional Be stock material and service to bond the window by a high-temperature braze process. Although the end products were functional, the cosmetic quality of the brazed windows was not equal to that which can be obtained by the electron-beam welding process. In addition, the magnitude of iron contamination in their Be stock was greater than desirable (approximately 500 ppm iron contamination).
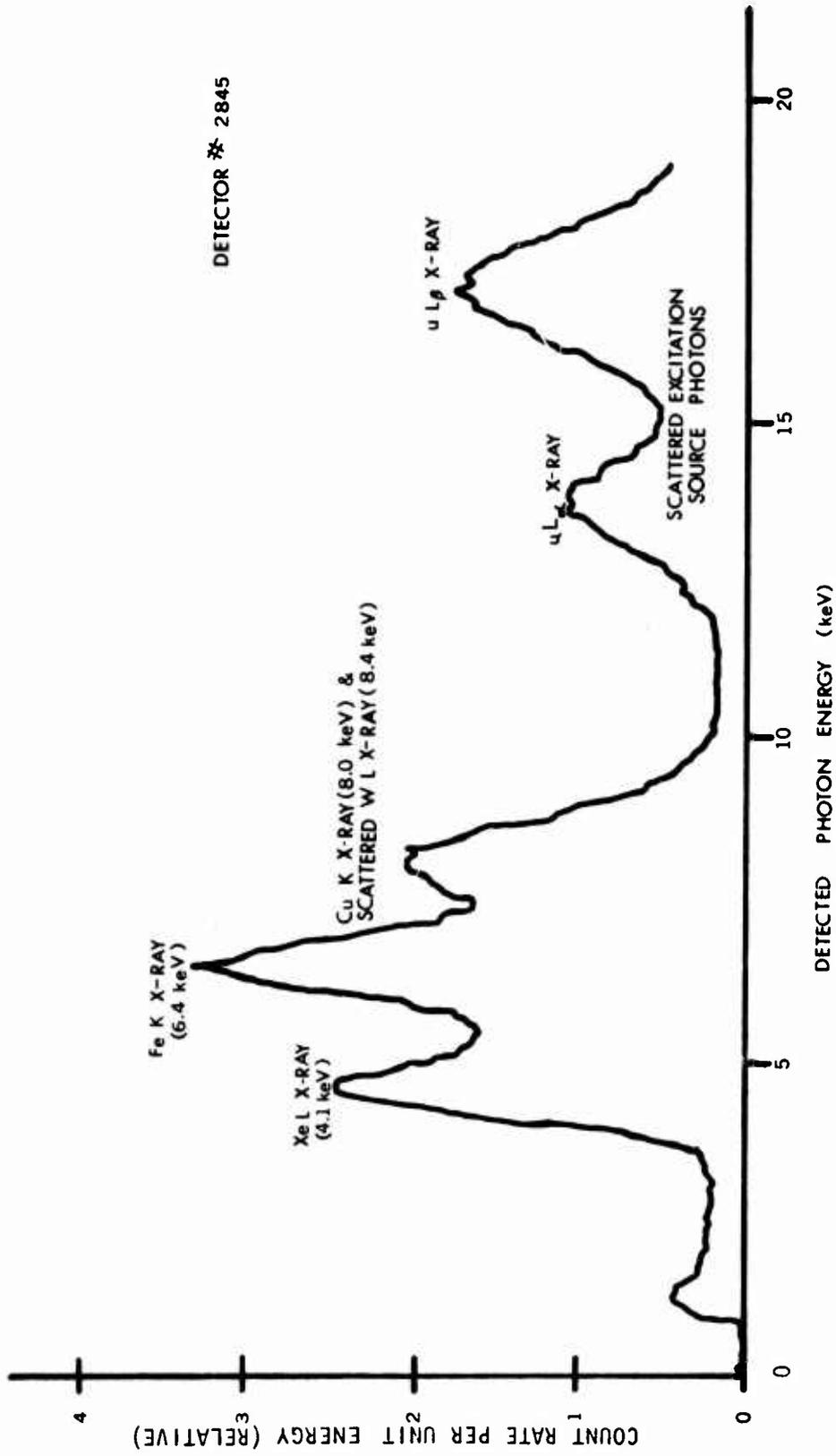
Figure 18. Detector Window Contamination – Improved Resolution.

34

The quality of beryllium used in the window can play a signifi-
cant role in establishing the lower limit of ODM sensitivity.
As previously indicated, gauge sensitivity is limited by the
background count rate. The magnitude of iron contamination in
the beryllium window directly affects the background count rate.
"Nuclear-Grade" Be is reported to have a maximum of 0.075%
iron[7]. Such a level would present a mass of 350 micrograms of
iron per square centimeter of window area. Through selection,
we were initially able to obtain 10-mil Be with iron contamina-
tion as low as 150 ppm. Figure 19 presents the spectral dis-
tribution from "Nuclear-Grade" material as compared to the high-
purity stock. The 10-mil window stocks were placed in a source-
detector geometry like that of the ODM to obtain the spectra of
Figure 19.

The oil pressure relief valve on the UH-1 transmission is set
to 50 psi. Thus, one can assume that the Be window will see a
maximum stress (Sm) at that pressure. For a thin, rectangular
plate which is fixed on all edges, maximum stress can be cal-
culated by an expression from Marks[6] which is

$$S_m = \frac{k\ w\ r^2}{t^2} \tag{8}$$

where k = empirical factor

               r = length of shorter side of rectangular
                    plate (inches)

               w = uniformly distributed load (psi)

               t = plate thickness (inches)

From Marks[6], K is 0.497 when Poisson's ratio is 0.3 and the
shorter side length (r) is half that of the longer side. For
the case in point, the dimensional relationship is appropriate;
however, Poisson's ratio is 0.03 and K is reduced by a factor
of 10. The ODM beryllium window has a t of 0.01 inch and an r
of 1.24 inches; the maximum probable load w is 50 psi. From
equation (8), S_m is evaluated to be 3.9×10^4 psi. Cross-
rolled Be exhibits yield and ultimate tensile strength of 6
and 8×10^4 psi, respectively[7]. From this, there appears to
be a safety margin of approximately 1.5

The magnitude of window overpressure is usually less than pre-
viously indicated. As discussed in the following section,
the technique for oil sampling provides a slight negative
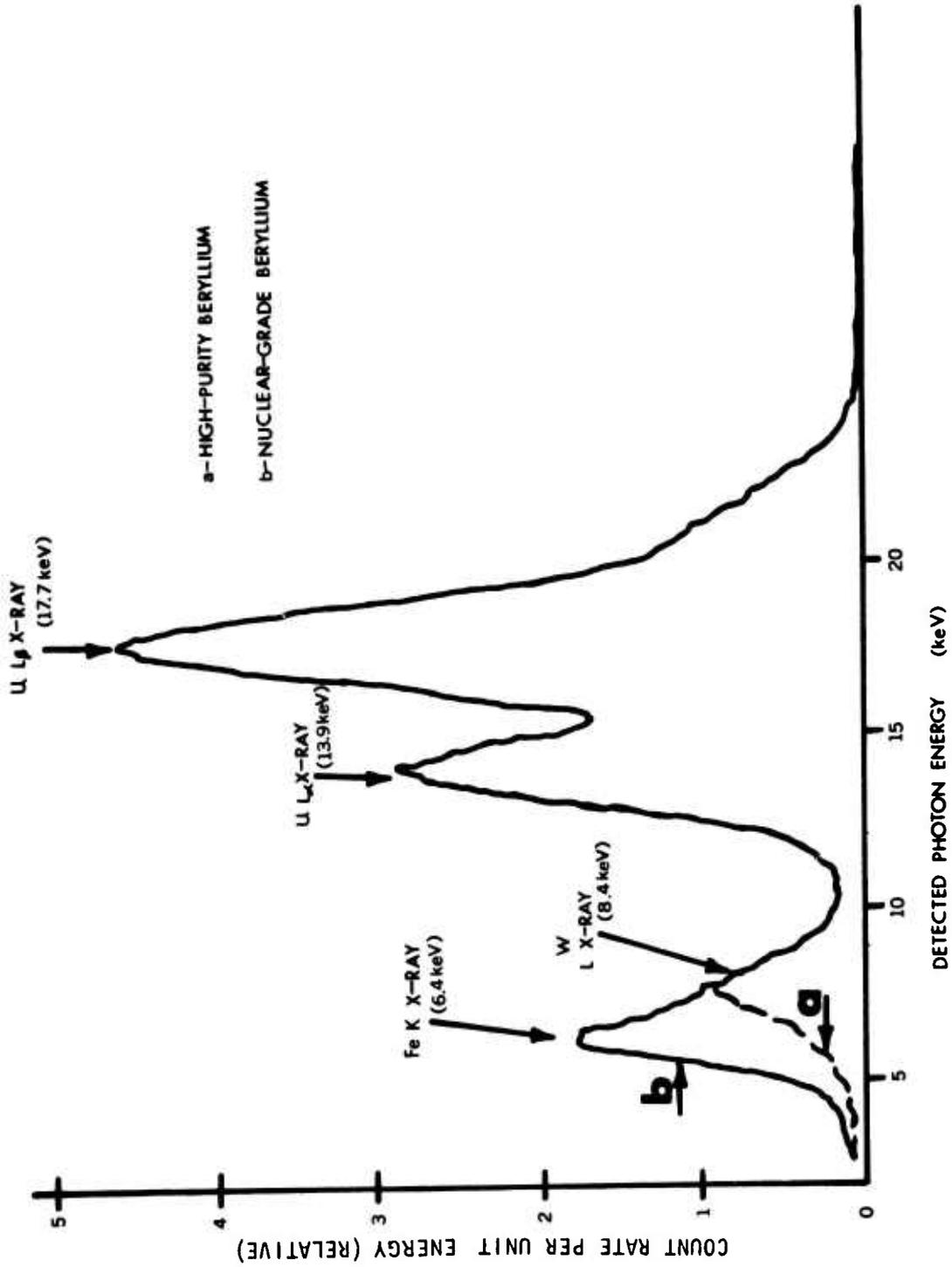
Figure 19. Flow-Cell Window Contamination.

pressure in the flow-cell during normal operations. Only a severe restriction at the 0.55-cm-diameter orifice plate or downstream from the cell could conceivably produce a pressure of 50 psi on the window.

3.4 OIL FLOW-CELL

In the ODM, the detected count rate from a nominal iron contamination level is small with respect to the total detected count rate. Hence, a long counting time (i.e., a large total count accumulation) is required to provide statistical significance to that small count rate fraction. This measurement characteristic was described in Section 2.0. If the gauge observes an iron mass of 400 micrograms during 1% of a measurement period and no iron for the remainder of that period, the resultant gauge output would be equivalent to a uniform iron mass distribution of 4 micrograms. Gauge performance such as this would obscure dynamic changes in lubricant quality and drive-train mechanical status. The two extremes in this factor of ODM design are that one can measure either the contaminant mass level within a large oil volume with a large measurement uncertainty or that within a small oil volume with a small measurement uncertainty. In an ideal case, the gauge's effective sample volume would be changed at a rate comparable to the gauge's measurement period.

The range of fluorescent X-rays in the oil medium defines the effective sample volume. This volume is very small ($<1cm^3$) with respect to typical lubricant volume flow rates (4-60 l/min). This difference in volume, coupled with the long measurement times (4-60 min), dictated the design criterion for the fluid sampling technique. A lubricant flow-through tube with orifice and upstream and downstream sample ports was incorporated into the ODM sensor head to satisfy this criterion. As fluid passes through the orifice restriction, its acceleration produces a pressure differential by the Venturi principle. This pressure differential is used to draw oil from the upstream sample port into the flow-cell and subsequently back out through the downstream sample port.

Qualitative preliminary testing involved visual observation of water, dyes and small suspended particles through a lucite flow-cell cover. Pertinent physical parameters (e.g., flow rate, orifice diameter, sample port size and location, etc.) were varied to establish an appropriate flow pattern and sample volume exchange rate. The final configuration is one where the flow-through tube has a 1-cm diameter and the orifice plate diameter is 0.55 cm. The sample inlet port is 0.16 cm in diameter and 5 cm upstream from the orifice. The sample exit port is immediately downstream from the orifice; it is a slot on the tube's circumference, 0.08 cm wide by 2 cm long.

37

The upstream port diameter (0.16 cm) provides an upper limit to the size of iron particles admitted into the flow-cell. The gravitational force exerted on a 0.16-cm-diameter iron particle is calculated to be 16.6 dynes. The drag which the oil presents to that particle is calculated to be 14.6 dynes. At low fluid flow rates, flow-cell circulation effectiveness can be influenced by gravity. To assure effective uniformity of the sample volume within the flow-cell, its placement attitude is on the horizontal plane with the source-detector volume located below the flow-cell.

The pressure differential Δp was calculated to be 2.303 g/cm^2 (2.257 x 10^3 dynes/cm^2) for a flow rate of 1 liter per minute. The pressure-flow rate relationship is described in the equation from Marks[6] as

$$\Delta p = \left[\frac{Q}{C_D A_O}\right]^2 \qquad \frac{\rho \, (1-\beta^4)}{2 \, g_n} \qquad g/cm^2 \qquad (9)$$

where $\quad$ Q = flow rate (cm^3/sec)

$\quad$ C_D = ratio of actual to ideal discharge through orifice

$\quad$ A_O = orifice area (cm^2)

$\quad$ ρ = fluid density (g/cm^3)

$\quad$ β = ratio of orifice diameter to tube diameter

$\quad$ g_n = gavitational acceleration (cm/sec^2)

In the evaluation of Δp, a value of 0.97 was used for C_D.

The sample volume exchange rate v is proportional to the pressure differential between the lubricant at the upstream port and the sample volume. The rate of volumetric exchange can be calculated by the expression[8]

$$v = \frac{p \, R^4}{8 T \eta} \qquad cm^3/sec \qquad (10)$$

where $\quad$ π = ratio of a circle's circumference to its diameter

$\quad$ Δp = pressure differential between fluid at the upstream port and sample volume (dynes/cm^2)

R = upstream port radius (cm)

T = tube wall thickness (cm)

η = coefficient of fluid viscosity (dyne sec/cm^2)

With this expression, v was calculated to be 2.72 cm^3/sec for a flow rate of 1 liter per minute. In the calculation of v, Δp was considered to be 1/8 of the total Δp, which is the ratio of the upstream sample port area to the area of the downstream port. A value of 1.25 x 10^{-1} dyne sec/cm^2 was used for the coefficient of fluid viscosity.

The sample volume exchange rate was measured experimentally by monitoring the ODM sensor output rate as a function of elapsed time after introducing a step change contamination level of dissolved iron to the ODM test loop. Figure 20 presents the sensor response at a fluid flow rate of 1.94 liters per minute. As shown in the figure, 80% of the equilibrium value was achieved within 14 minutes. Theoretical calculations indicate a fractional equilibrium of 76.9% in 14 minutes.

As shown by Figure 20, the iron contamination level in the flow-cell exibits an asymptotic exponential response to a step change in the level of contamination within the total lubricant system. This characteristic is analogous to a resistive-capacitive response to a step change in voltage and the diffusion of heat, pressure, or chemical concentration between two finite volumes separated by a semipermeable barrier.

Although the flow-cell contains 160 cubic centimeters (nominal), the sensitive volume is far less than this. Tests were performed to ascertain the geometric response of the sensor. Figure 21 shows the sensor's response to an iron particulate mass in the plane adjacent to the beryllium window. The data of this figure are normalized to the 1/4-inch grid having the highest count rate with the maximum rate set equal to 100. From these test data, it is apparent that only the area in close proximity to the Pu-238 excitation source provides a significant XRF contribution. Figure 22 presents data of the sensor response as a function of oil thickness between the iron mass and the window. From these data groups the effective oil volume was determined to be 0.324 cubic centimeter.

Additional tests were performed to evaluate the effect which oil depth has on the background count rate in the energy region of the iron X-rays. Figure 23 illustrates this effect; it is caused by the increased mass acting as a scattering source. The undesirable increase in background count rate is offset in part by an increase in XRF yield. This is brought about by an increased excitation source flux within the

39
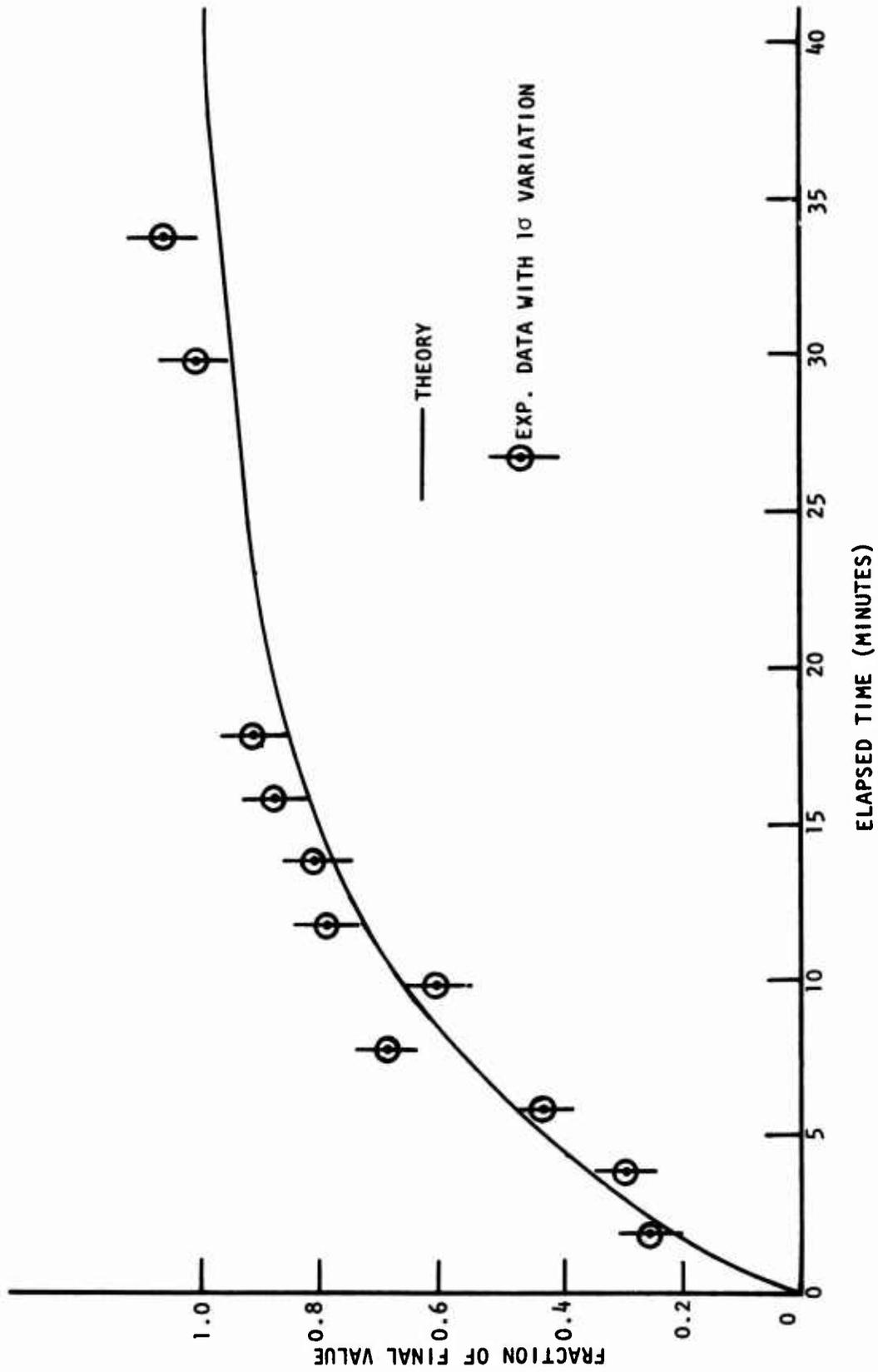
Figure 20. Dynamic Response of Flow-Cell Sample Function.
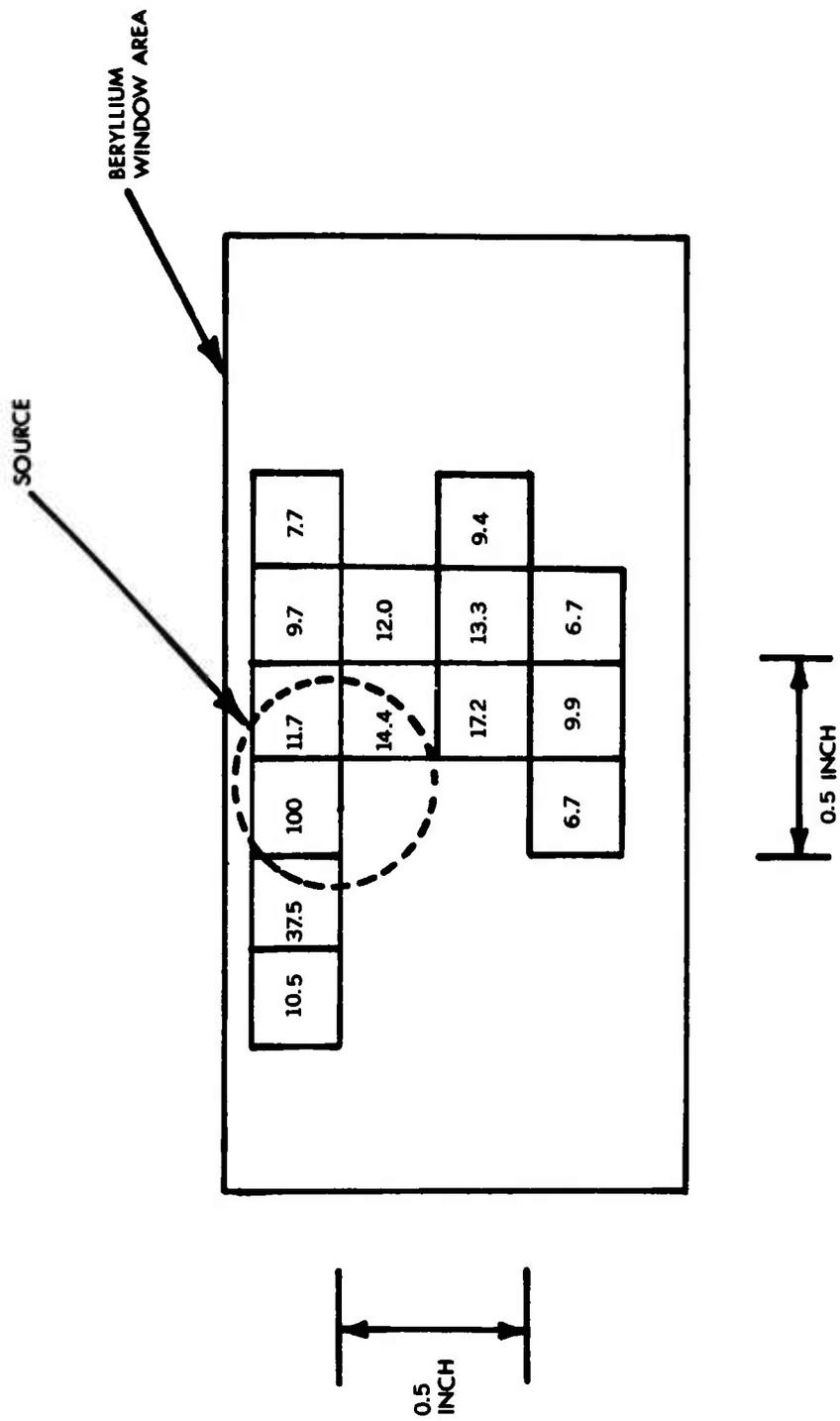
Figure 21. Sensitive Sample Areas of Flow-Cell.
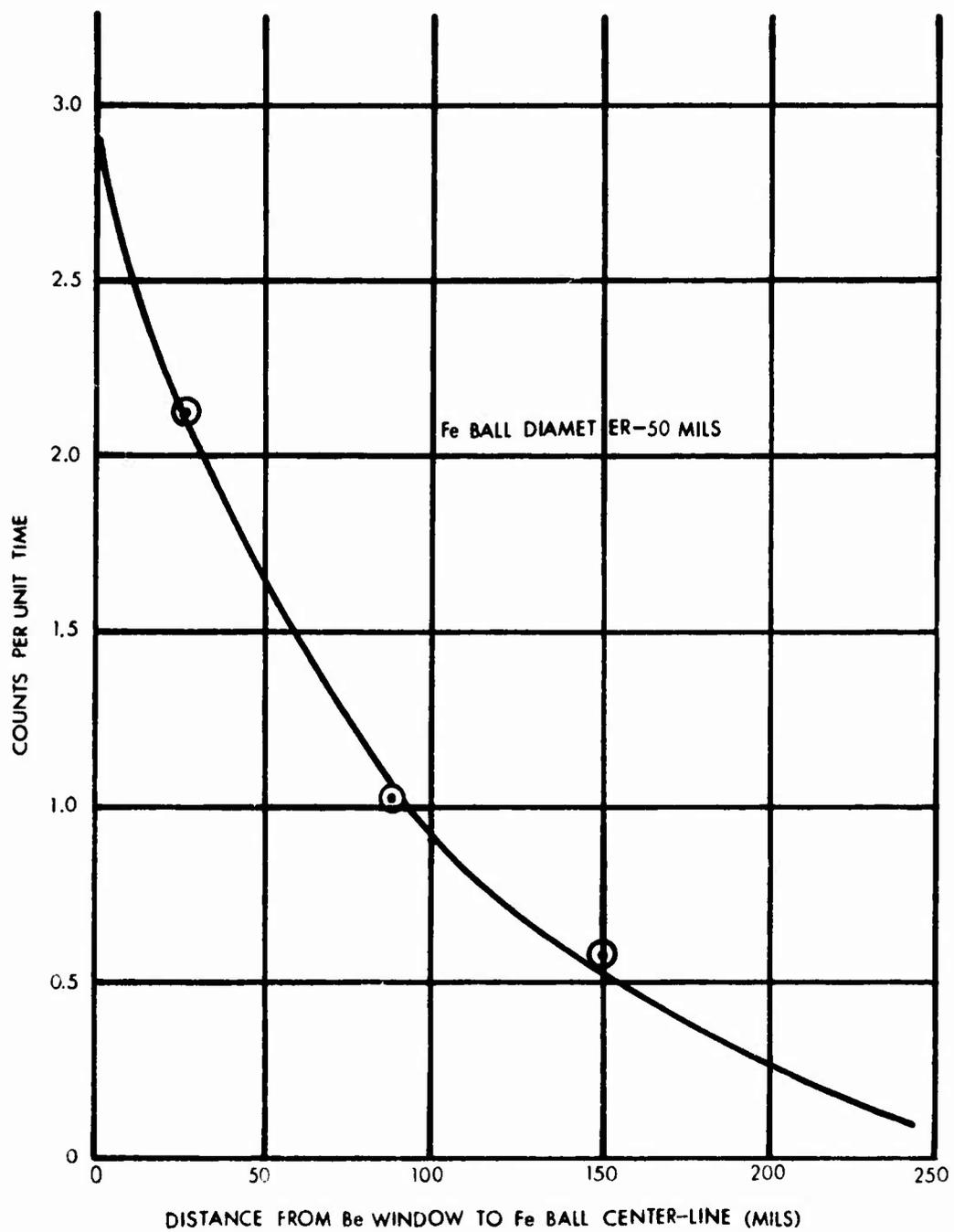
Figure 22. Sensitive Sample Height of Flow-Cell.

42
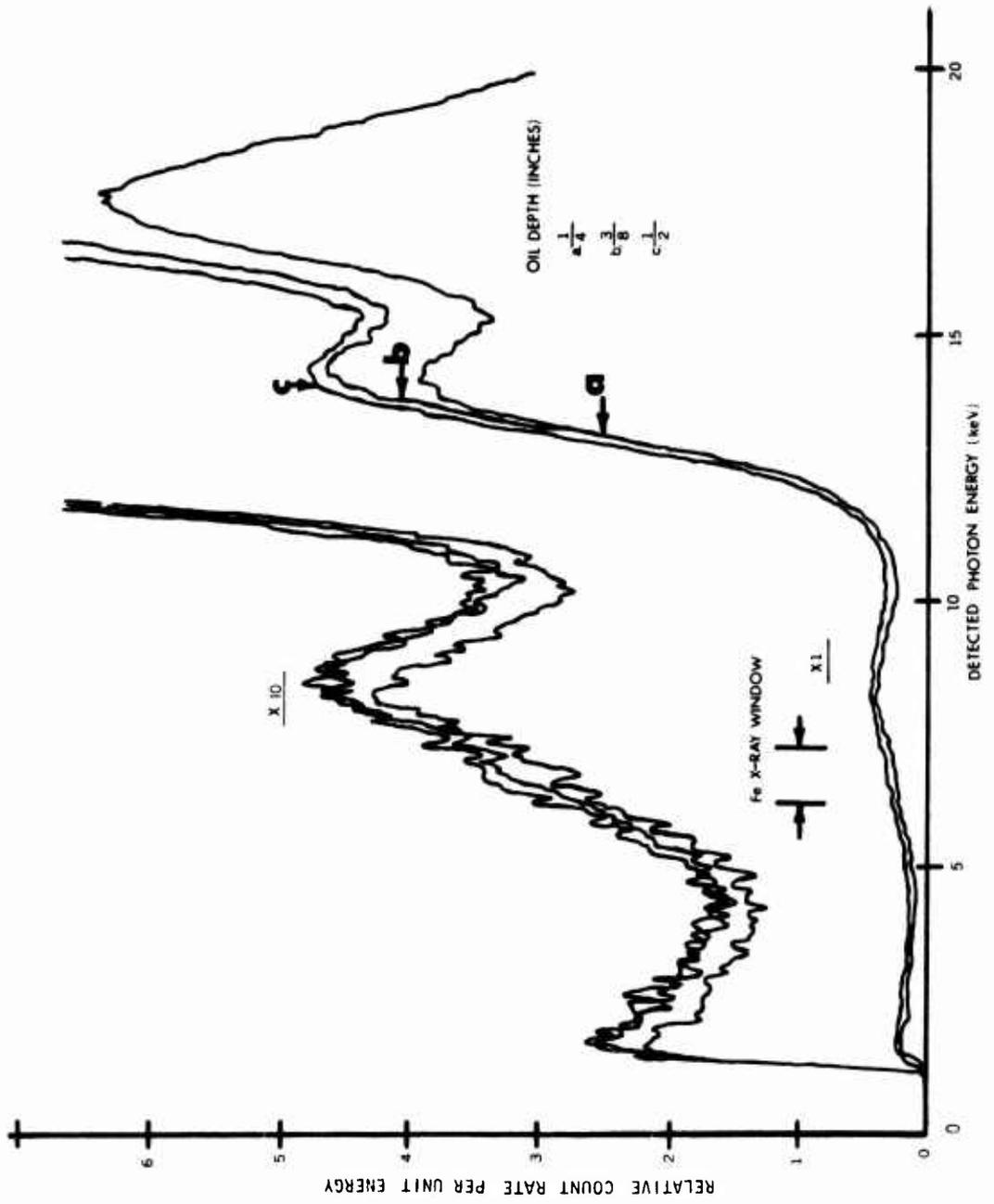
Figure 23. Background Spectra vs Oil Height.

effective oil volume; the effect is analogous to an increase in the excitation source's emission rate. Table II lists count rate data of the Fe X-ray energy region for the spectra of Figure 23 as well as that for a contamination level of 30 ppm Fe (nominal) under the same conditions. As the oil depth increases from 1/4 to 3/8 inch, the background increases by 14.5% and net XRF increases by 20%. Figure 24 illustrates the energy spectra for 0 and 30 ppm at the 1/4- and 3/8-inch oil depths.

3.5 TEMPERATURE EFFECTS

The ODM is intended for operation with oil at temperatures ranging from $100°F$ to $300°F$. In MIL-L-7808 oil, the specific gravity will change from 0.929 to 0.891 gram per cubic centimeter during that temperature change. There are changes in radiation scatter and attenuation characteristics brought about by this density change since it is effectively a change in mass per unit area presented to the source-detector assembly.

The data presented in Section 3.4 give indications as to the multiple photon-oil interaction phenomena; a change in oil density has the same effect as a change in oil depth. Figure 22 shows that the effective oil depth for the Fe X-rays is approximately 0.2 inch, which is the effective saturation thickness. Thus, any change in oil depth beyond the saturation thickness will have no effect on detected Fe X-ray intensity when the excitation source flux remains constant. However, the excitation source flux within the oil volume is subject to minor variations.

Approximately half of the excitation photons pass through the oil volume and interact with the aluminum housing. A small fraction of these interactions cause photons to scatter back into the oil volume; this scatter intensity remains essentially constant as the oil temperature and density change. Excitation photons scatter in approximately 32% of the photon-oil interactions - a factor of 5.7 greater than in aluminum. The photon-oil scatter rate decreases by 2.5% as the oil temperature goes from $100°F$ to $300°F$. Hence, the effective excitation source photon flux in the oil decreases by that amount. The Fe X-ray production is a direct function of the excitation source flux intensity. Therefore, it will also change in a similar manner.

By necessity, the radiation detector is in close proximity to the oil volume and therefore is exposed to heat radiated through the beryllium window and the adjacent aluminum. Proportional counter tube gain and resolution are both affected by temperature. The AGC circuit provides control for the detector bias to prevent gain changes induced by either count rate or temperature. There is no effective countermeasure to negate the temperature effect on detector resolution.
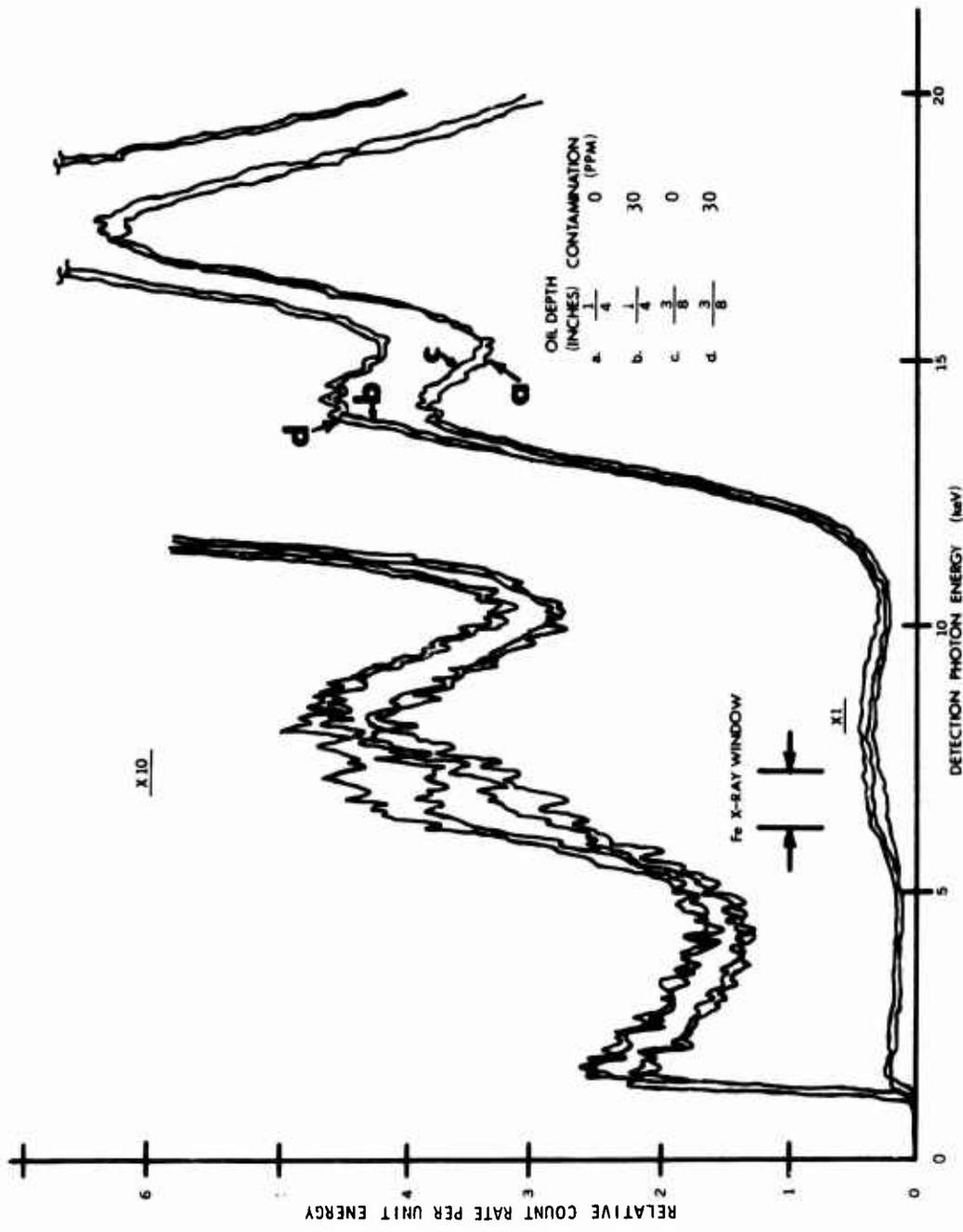
Figure 24. Spectra From Contaminated/Clean Oil.

TABLE II. IRON X-RAY COUNT RATES		
	Fe Count Rate (Counts/Second)	
Oil Depth (Inches)	Clean Oil	30 ppm Fe Contamination
1/4	186.53	232.34
3/8	213.56	268.51
1/2	221.35	
1/2*	219.36	
* Flow-cell cover in place.		

With the ODM hardware, it was observed that detector resolution
improved as tube temperature increased throughout the range of
interest. If the instrument's electronic pulse height analysis
(PHA) window is set to include the total Fe X-ray peak width
for a tube resolution of 20%, the detected iron count rate will
not change as resolution improves, such as a resolution chang-
ing from 20% to 18%. If the PHA window is set to a width less
than the total peak width, the detected iron count rate will
increase with resolution improvement. For example, consider a
window set to the full width at half maximum peak height (FWHM)
for 20% resolution. When the resolution improves to 18%, the
detected iron count rate as outputted from the PHA would in-
crease by 6.4%. The detected fraction of the Fe X-ray peak
population would go from 75% to 79.8%, which produces a count
rate ratio of 1.064. Thus, it would appear that the PHA window
would best be set to the full peak width. Such is not the case
from the standpoint of improving the signal-to-background ratio
(discussed in Section 2.0).

Figure 25 shows the fractional sample population of a gaussian
distribution as a function of width (σ) about the most probable
value. This statistical model is an appropriate representation
of the PHA window width with respect to a detected X-ray peak
where σ is the standard deviation of the pulse height distri-
bution. From the curve it is apparent that a total width of
6σ is necessary to include 99% of the population. A value of
2.35σ is equal to the FWHM and contains 75% of the population.

The common detected background energy distribution is a slowly
varying continuum and may be considered to be constant over the
energy range of interest. Hence, a change in PHA window width
from 6σ to 2.35σ will reduce the continuum background contri-
bution by 61% while reducing the sample intensity by only 25%.
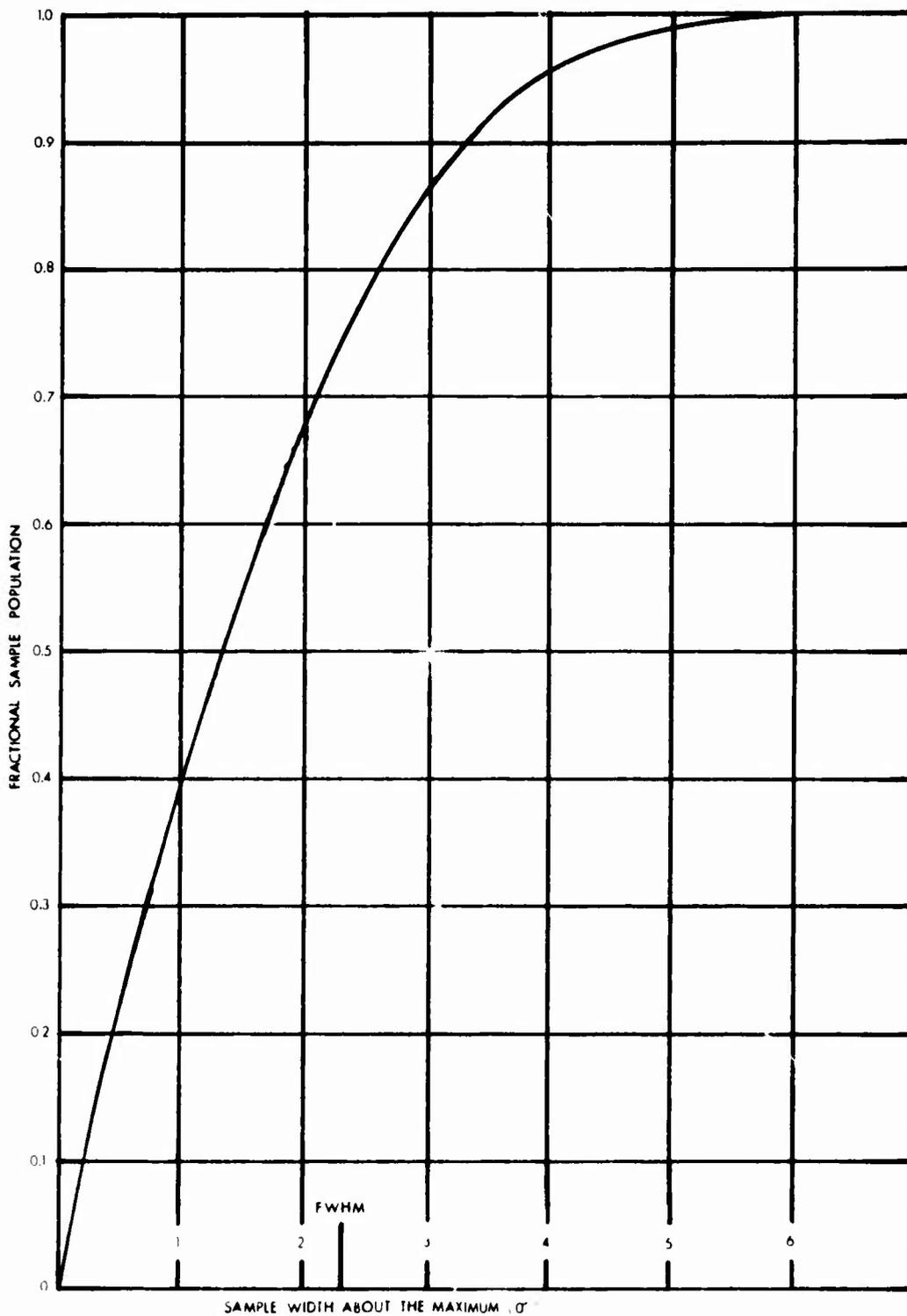
Figure 25. Detected Event Fraction vs PHA Width.

47

Thus, there are conflicting considerations and performance trade-offs with respect to selecting an appropriate PHA window width.

One additional factor warranting consideration in the selection of PHA window width is the existence of another X-ray peak near the one of interest. Such is the case in the ODM. The detected Fe X-ray distribution is partially overlapped by the detection of scattered 8.4 Kev L X-rays from tungsten, the shield material in the plutonium source capsule. The tungsten XRF background distribution changes with temperature. Its scatter intensity decreases as oil temperature increases and density decreases. Its detected energy distribution (i.e., resolution) will also improve with temperature. Hence, the background contribution from these L X-rays in the Fe X-ray energy window will be reduced as temperature increases.

The preceding discussions have described how oil temperature changes are detrimental to optimum ODM performance. After consideration of those factors, corrective measures were employed to minimize those temperature effects.

The PHA window width was set equal to the FWHM of the detected Fe X-ray peak at an oil temperature of $100^{\circ}F$ to maximize the signal-to-background ratio. Subsequently, a temperature compensation factor was applied electronically to the ODM measurement period control. Compensation was accomplished by routing a reference voltage through a platinum resistance temperature sensor in the oil flow-cell and into a voltage-to-frequency converter (VFC). The VFC output was then used as the primary clock frequency for controlling the ODM measurement time periods. Figure 26 shows the change in primary clock frequency as a function of oil temperature. The measurement time period increases by approximately 0.5% from ambient temperature to $300^{\circ}F$.

The effectiveness of the temperature compensation is illustrated in Figure 27, which presents ODM output in consecutive 5-minute measurement periods during which the oil temperature was varied over the temperature range of interest. The ODM had previously been calibrated at $100^{\circ}F$ with a nominal contamination level of 100 ppm. Throughout the 95-minute period shown in the figure, the average temperature was $200^{\circ}F$ and the average ODM output indication was 104 ppm. Considering a 2σ statistical uncertainty of 10 ppm, the agreement is reasonable. It appears that these ODM data indicate a minor tendency to error slightly on the high side at the higher temperatures. If statistical considerations are excluded, the data of Figure 27 could be interpreted as showing a positive gauging error of 4% per 100 degrees change in oil temperature. This gauging error estimate is believed to be a reasonable limit of the measurement uncertainty caused by changes in oil temperature.

48
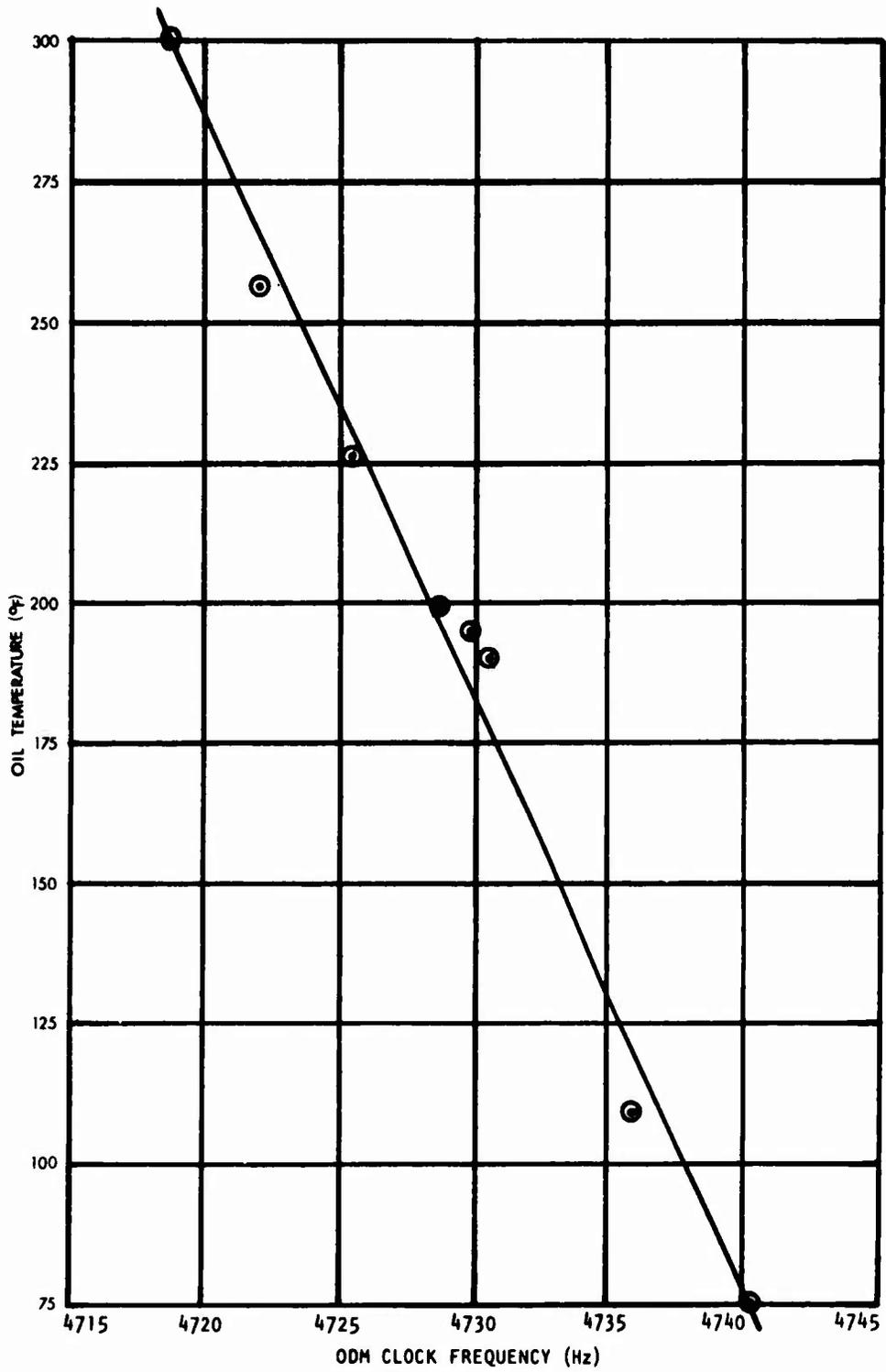
Figure 26. Oil Temperature Control of Clock Frequency.
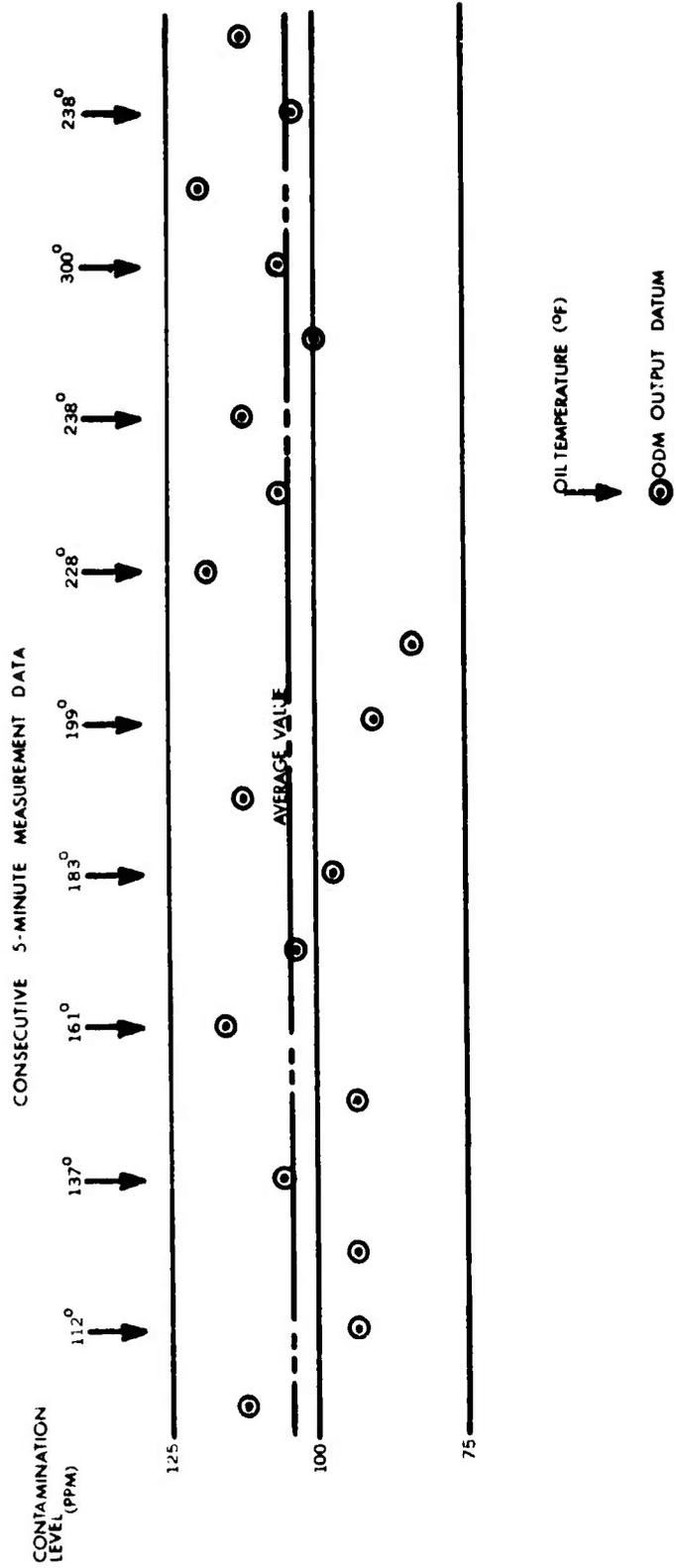
Figure 27. ODM Response During Changing Oil Temperature.

4.0 ODM SYSTEM DESIGN AND PERFORMANCE

The Model 003 oil debris monitor is designed for quick and easy installation and simple, unattended operation. It will interface conveniently with test cell setups on both the UH-1 transmission and the 90° gearbox. Although there is reasonable technical sophistication in its gauging physics and electro-mechanical design, personnel can take advantage of the ODM's capabilities without a detailed knowledge of those disciplines or the instrument itself.

4.1 ELECTROMECHANICAL CONFIGURATION

The ODM consists of a probe, amplifier box, and electronic instrument. These components are stored in an aluminum carrying case having less than 1 cubic foot volume. The case has an outside fitting cover which is hinged and removable from the box. The cover has an inner lid storage compartment in which the AC power cable, instrument interconnect cord, probe and amplifier box are stored. The box serves as a housing for the electronic instrument. This unit is illustrated in Figure 28.

The probe contains the oil flow-cell, oil temperature sensor, and radiation source and detector. The overall dimensions of the probe are appoximately 3 by 6 by 7 inches. Cables from the temperature sensor and the radiation detector are joined to the amplifier box. These cables are approximately 2 feet long.

The amplifier box is approximately 4-1/2 by 3-1/2 by 3 inches in size; it contains three electronic modules. The first amplifies a DC voltage (6-12 volt input, 1200-3200 volt output) to provide the appropriate voltage potential to the radiation detector. The other modules amplify and shape the charge impulses output from the radiation detector. Power, ground, and signal cables within the instrument interconnect cable join the amplifier box to the electronic instrument. This cable is nominally 6 feet in length. The ODM with its cables attached is illustrated in Figure 29.

The instrument panel, illustrated in Figure 28, has two meters for visual indication of output and output terminals to permit remote monitoring or recording of ODM readout data. Interconnect cable and AC power cable connectors and the STATUS switch are also located on the panel. Access to the PC boards and calibration controls is obtained through the hinged panel adjacent to the instrument panel, as shown in Figure 30.
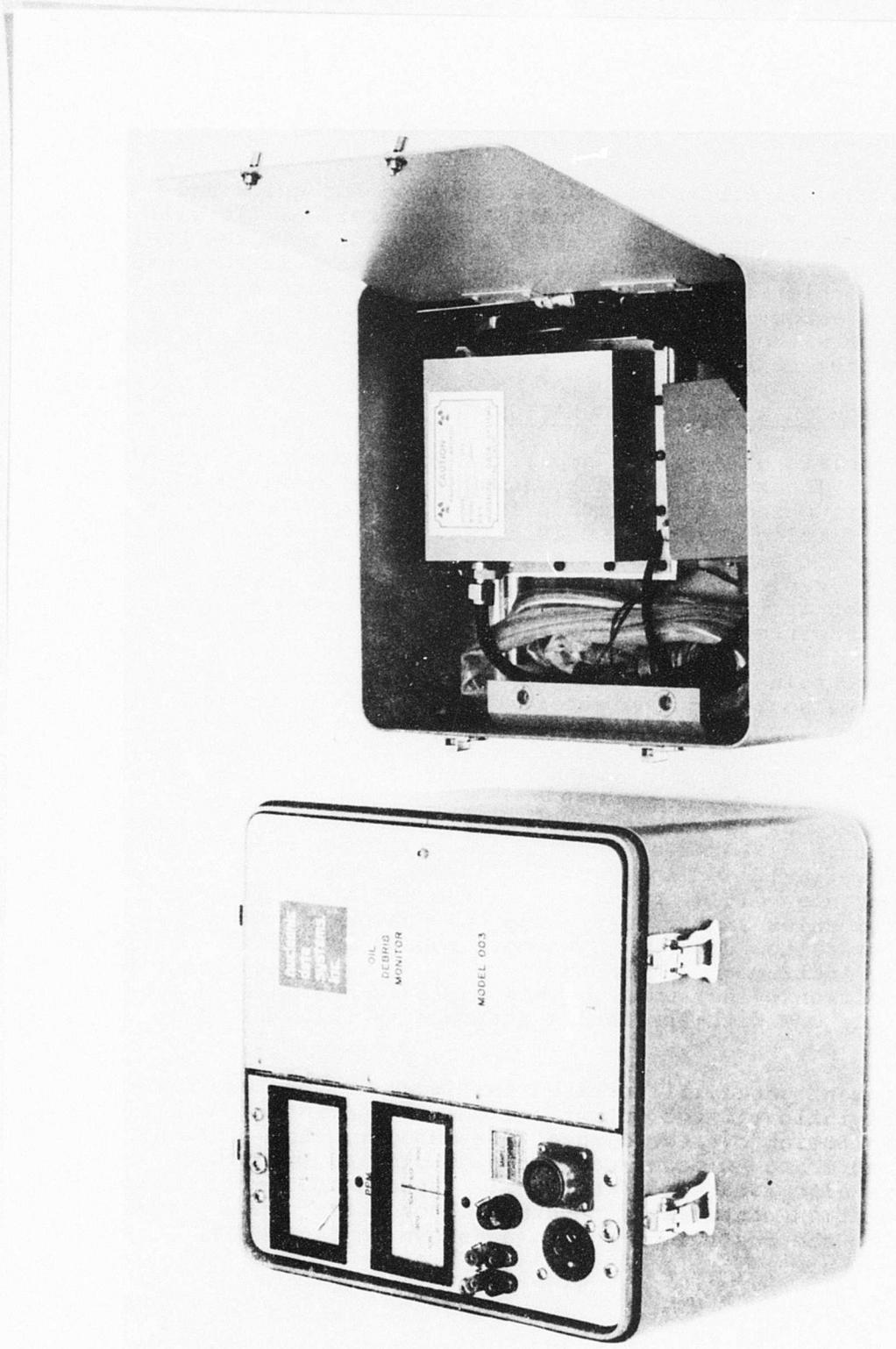
Figure 28. ODM and Lid Storage Compartment.

52
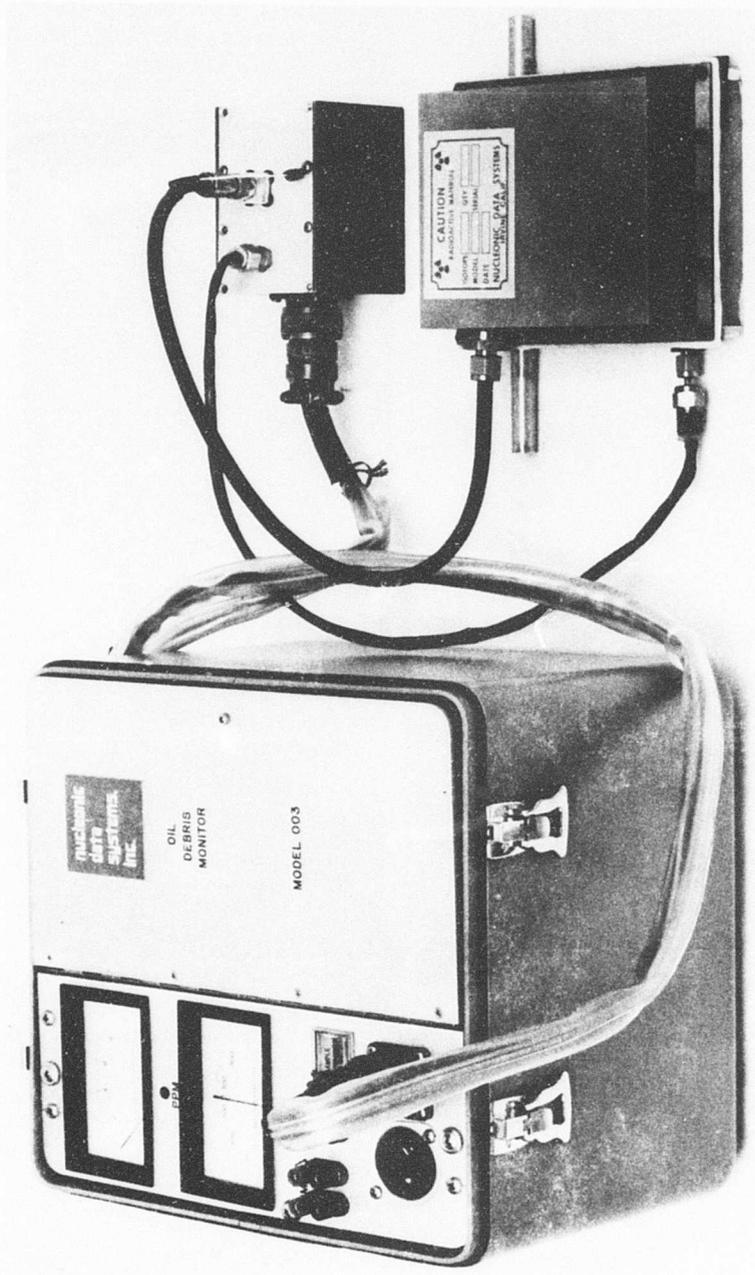
Figure 29. ODM With Cables Connected.

53
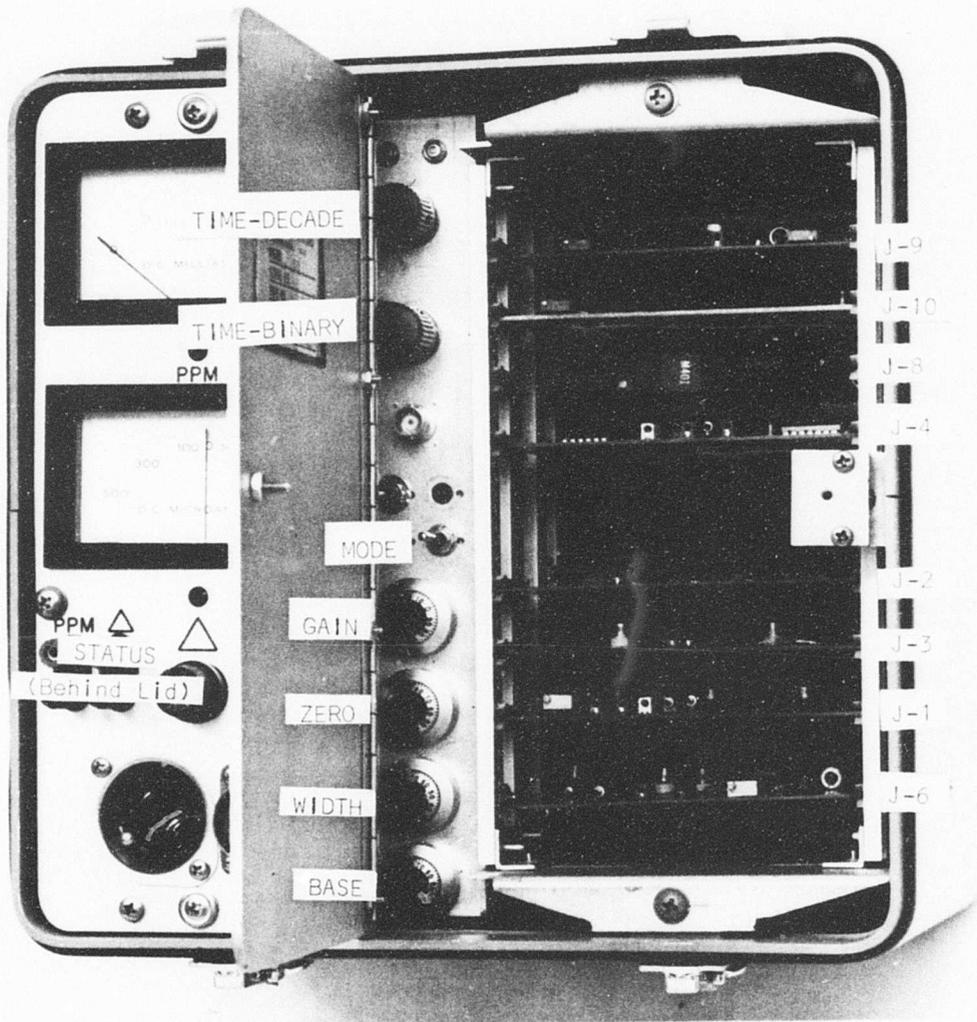
Figure 30. Hinged Access Panel.

The ODM flow-cell can be mechanically interfaced with the oil
line in either of two general ways. These are illustrated
schematically in Figure 31(a) and (b). In the first, interface
flow-cell inlet and outlet parts (1/2-inch OD aluminum tubing)
are fitted with swagged locknuts. The parts are oriented such
that the cell can be replaced by a single, straight, 9-1/2-inch
length of tubing having like fittings. This connection offers
simplicity and ease of installation, particularly where space
is limited. An alternate interface geometry includes ancillary
hardware to allow uninterrupted fluid flow while the flow-cell
is removed, cleaned or serviced. A two-way gate valve directs
fluid flow through either the ODM cell or the bypass line. A
check valve prevents backflow to the cell when the bypass is
employed.

The ODM flow-cell has been designed to continuously sample a
small fraction of the lubricant as it passes through the cham-
ber. This is accomplished through placement of an orifice plate
in the flow-through oil tube and taking pressure taps upstream
and downstream from the orifice. The pressure differential
between these taps provides a continuous exchange of fluid be-
tween the oil line and the cell's sample volume. The flow-cell
holds an oil volume of approximately 160 milliliters. The down-
stream pressure tap (i.e., the flow-cell's sample exit port) is
a rectangular slot extending o ver half of the tube's circumfer-
ence to prevent entrapment of air, lubricant, and particles.

At oil flow rates greater than 10 gallons per minute (nominal),
sample exchange effectiveness should not be significantly in-
fluenced by gravity; hence, cell placement attitude is not
critical. At lower flow rates, effective sampling is best
achieved by cell placement on the horizontal plane with the
source-detector volume placed below the flow-cell.

Placement of the amplifier box and electronic instrument is not
critical. The 2-foot and 6-foot cable lengths from the ampli-
fier box to the flow-cell and the electronic instrument, respec-
tively, allow reasonable freedom in location and orientation of
these subassemblies.

4.2 FUNCTIONAL DESCRIPTION OF ELECTRONICS

Figure 32 is a functional block diagram of the different boards
and system components contained in the ODM. The function of
the different boards may be easily understood since all the
functions of one board are integrated into the schematic symbol
for that particular board or component. Where applicable, the
board number is also shown in order to facilitate identifica-
tion of that particular board in the instrument.
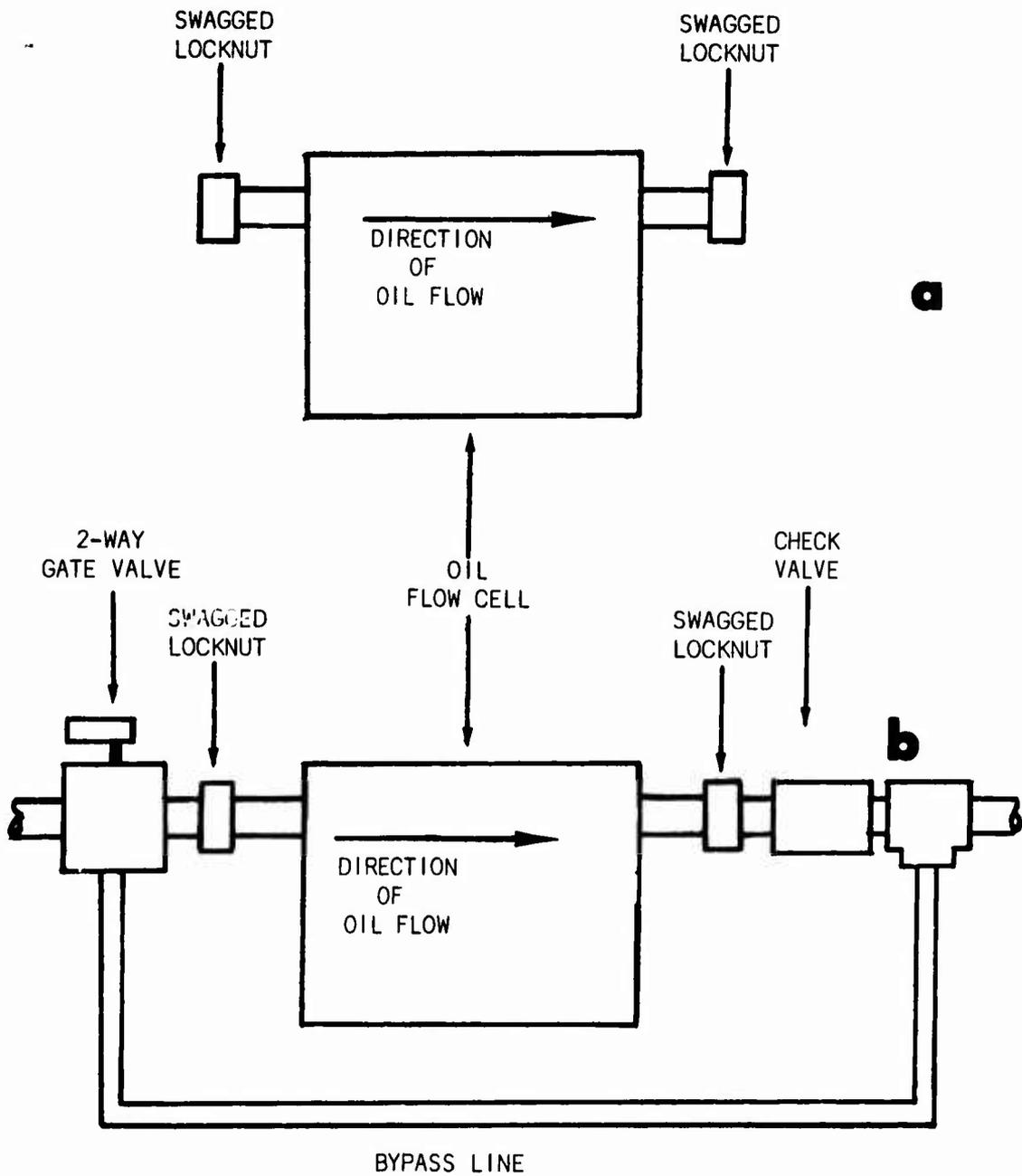
Figure 31. ODM Mechanical Installation Schematic.
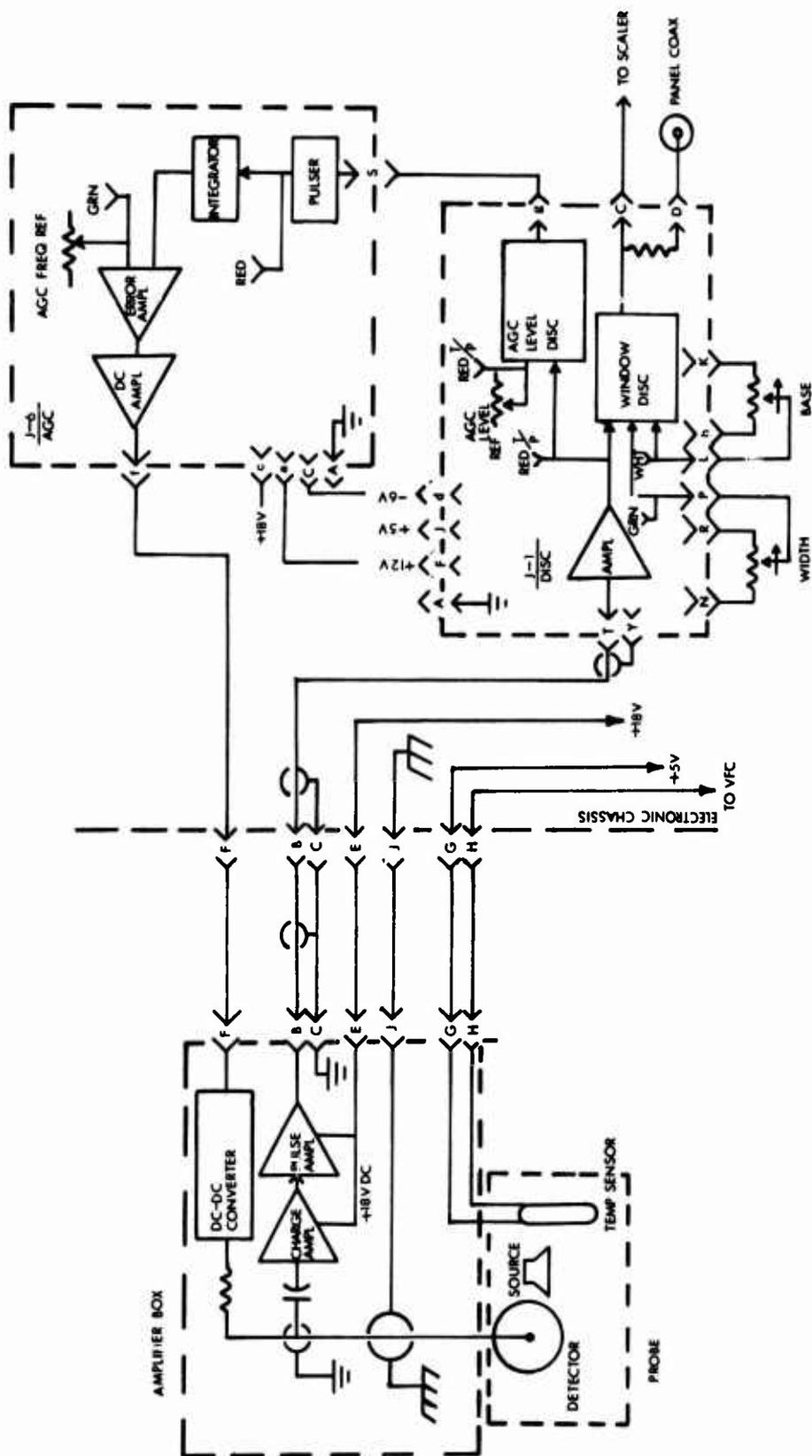
Figure 32. Electronics Functional Diagram (Sheet 1 of 3).
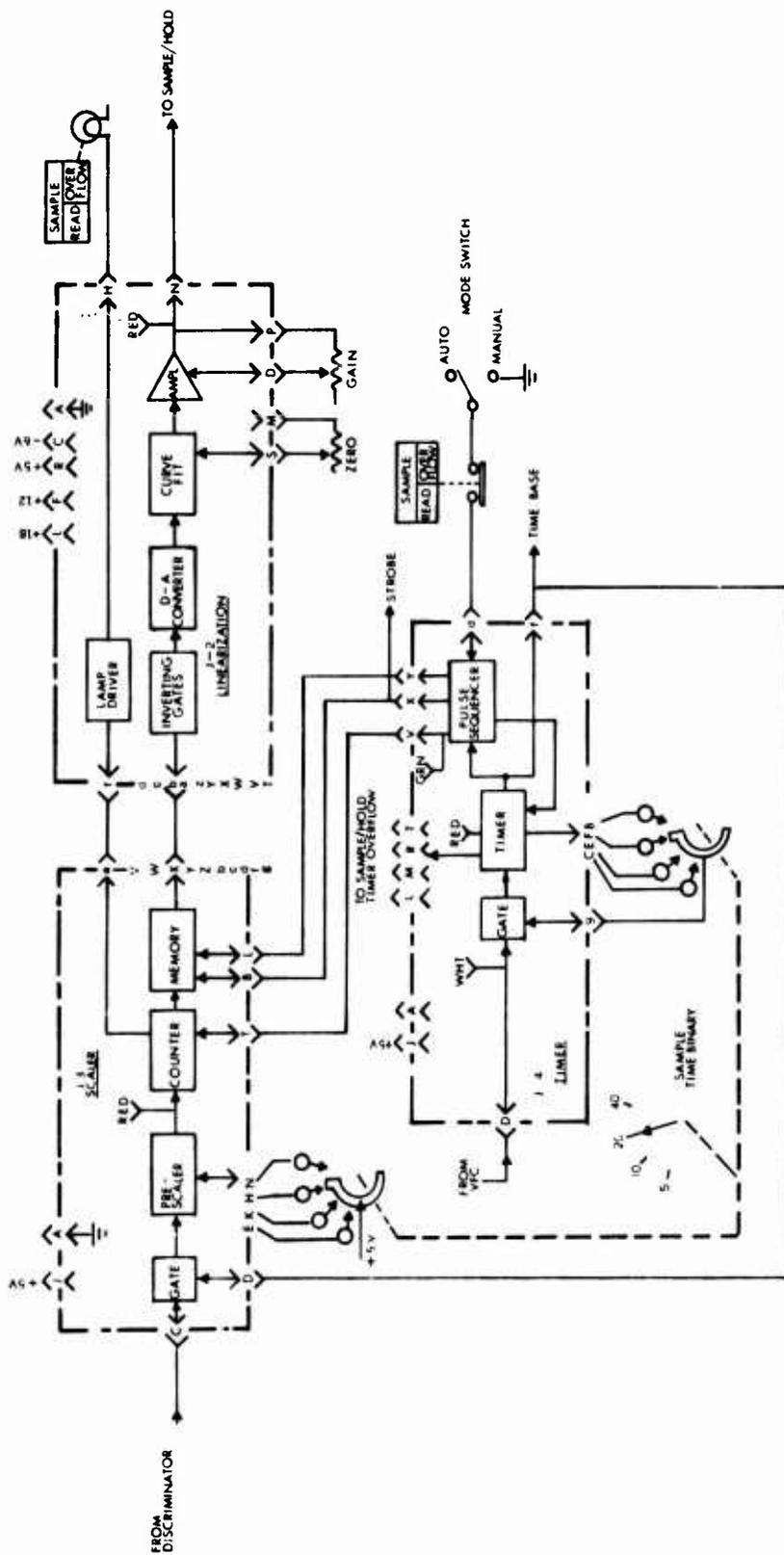
Figure 32. Electronics Functional Diagram (Sheet 2 of 3).

58
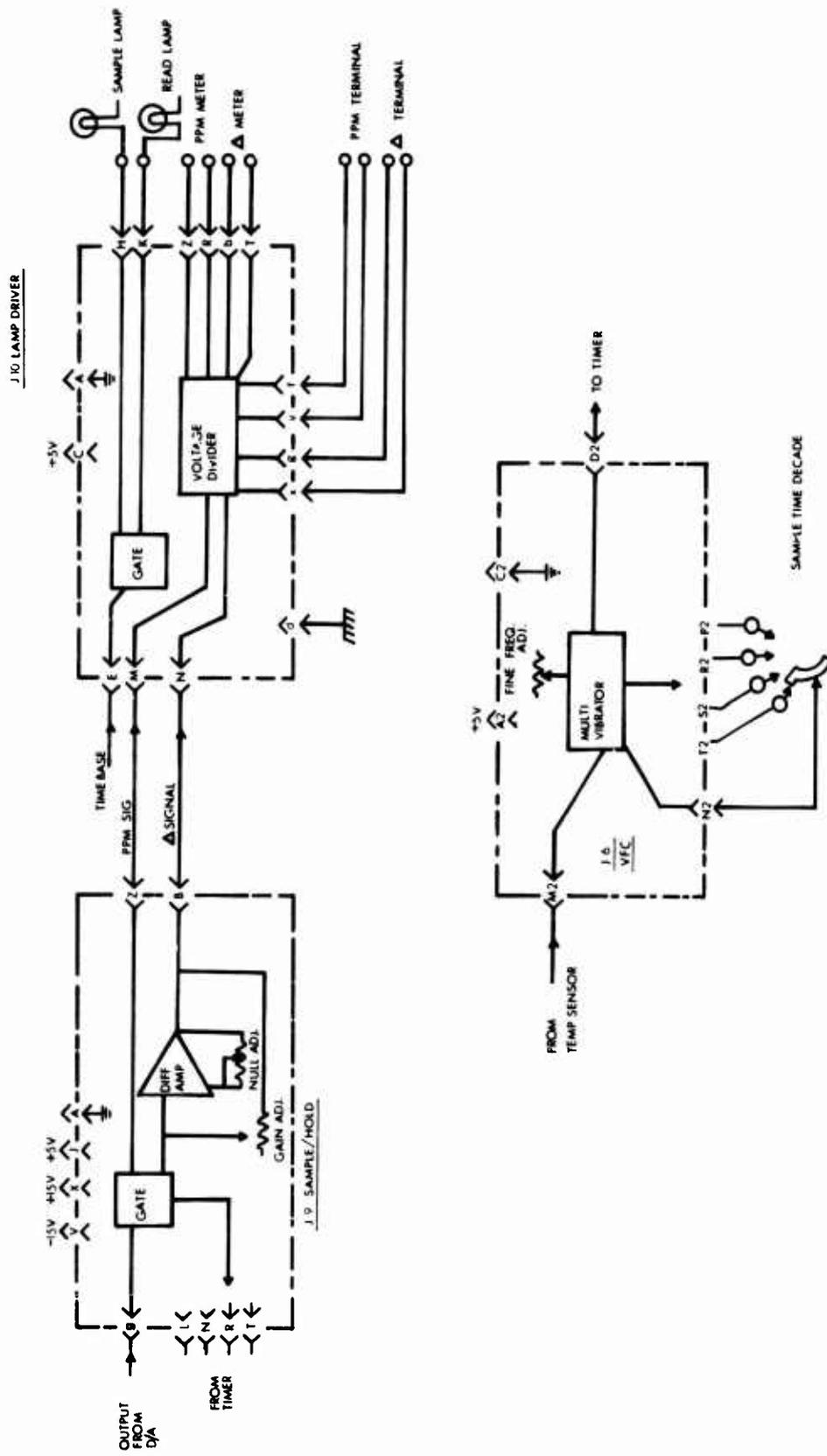
Figure 32. Electronics Functional Diagram (Sheet 3 of 3).

Positive-going tail pulses on the detector's triaxial HV cable are input, shaped and amplified through amplifier boards inside the amplifier box. The amplified analog pulse train is then transmitted to the instrument via a coaxial cable.

The discriminator selects pulses within the appropriate X-ray energy region as determined by the WINDOW BASE and WINDOW WIDTH control settings. Every input pulse within these defined limits provides a standard output pulse which is routed to the scaler board. These standard pulses are also available at the BNC connector on the inner control panel for use with an external scaler. Another threshold on the discriminator board supplies the standard pulses for the automatic gain control (AGC). The AGC contains a count rate integrating circuit which gives an averaged DC output voltage that is proportional to the incoming rate. This voltage is compared to a standard reference voltage. The voltage difference is amplified and routed to the DC/DC converter which produces the high voltage for the radiation detector.

A positive voltage (5 volts DC) is routed through the flow-cell's platinum resistance temperature sensor to the voltage-to-frequency converter (VFC) board. This voltage input and the SAMPLE TIME-DECADE switch position determine the output repetition rate of an RC-coupled multivibrator in the VFC. The VFC output pulse train serves as the primary source of timing signals in the digital circuits of the ODM. Fine frequency adjustments to this source are made with a potentiometer mounted on the VFC board.

The timer board accepts the VFC output pulses and provides the digital logic to produce gate, strobe, and reset pulses in a sequence appropriate to the ODM operational status. Timer performance is also subject to the position of the SAMPLE TIME-BINARY, MODE and STATUS switches.

The scaler counts the discriminator's output pulses for a time period determined by SAMPLE TIME switches (BINARY and DECADE). The timer gates the scaler for the time interval selected. At the end of the measurement, the scaler content is transferred to the memory. The memory is then read out by the digital-to-analog converter (D/A) board. This circuitry also linearizes the count rate dependence to the various gauging parameters to obtain a linear output signal response. The two display controls (WIDTH and BASE) allow for calibration adjustment.

The D/A board's output is proportional to the contamination level measured during the last completed sample time period. This output is routed through the SAMPLE/HOLD board to the PPM analog meter and terminal. While the analog signal is at the SAMPLE/HOLD board, its level is sampled and stored to allow for

comparison with the level of the subsequent measurement period. This comparison performs the function of evaluating the sequential change in contamination level during each successive measurement period. The SAMPLE/HOLD board's output goes to the PPM analog meter and terminal.

The LAMP DRIVER board serves the principal function of gating the lamp power to the STATUS indicators as determined by the level of TIME BASE logic signal. This board also has voltage divider and impedance matches for the four ODM signal outputs.

The DC voltage requirements of the ODM are served by four AC/DC converter modules. Two of these provide dual voltages. The module outputs include +18, +15, +12, +5, -6 and -15 volts DC. The placement of these modules is illustrated in Figure 33.

4.3 ODM OPERATION

Knowledge of three ODM controls is needed to operate the instrument. Controls important to ODM operation are:

1. SAMPLE TIME-BINARY (Rotary Selector Switch)

2. MODE (Toggle Switch)

3. STATUS (Push-button Switch)

The SAMPLE TIME-BINARY and MODE controls are located behind the hinged panel, as indicated in Figure 30. The STATUS switch is clearly illustrated in Figure 28 (located on the instrument panel).

As the SAMPLE TIME-BINARY switch is rotated clockwise (CW), the ODM measuring period changes from 5 to 10, 20, and 40 minutes (nominal) in sequence. Selection of a given measurement period involves consideration of the flow rate through the drive train's lubrication system, probable rate of change in the level of contamination within that system, and the ODM accuracy. If the primary interest is in observing very rapid changes in contamination level, the shortest measuring period would be used. System flow rate governs the sample volume exchange rate. Hence, a 5-minute measurement period is inappropriate if only a small fraction of the flow-cell oil volume has been exchanged during that period. Although the data presented in Figure 20 were taken for another purpose (i.e., evaluation of sample volume exchange), the indicated changes in contamination level as a function of elapsed time would be substantially different if a 40-minute measurement period was used. As discussed in Section 2.0, gauge accuracy is governed by the statistical uncertainty associated with the total count accumulation. If one changes the measurement period by a factor of 2 or 4, the accuracy will change by the square root of that factor. For
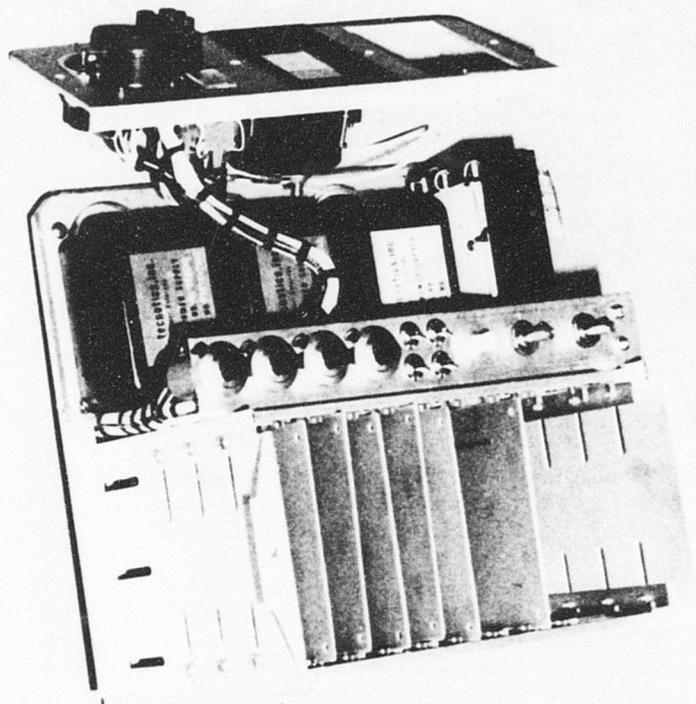
Figure 33. AC/DC Converter Placement.

example, the accuracy of a 20-minute measurement is one-half that of a 5-minute measurement (i.e., a factor of 2 better) and 1.4 times greater than that of a 40-minute measurement.

When the MODE switch is toggled toward the PC boards, the instrument operates in the AUTOMATIC mode and the measurement cycle is automatically repeated. When it is toggled in the opposite direction (MANUAL mode), the measurement cycle requires manual initiation by momentarily depressing the STATUS switch.

The unit requires a warm-up period of two measurement cycles when power is initially applied; the STATUS switch usually indicates an OVERFLOW condition during the initial measurement cycle. The initial ODM outputs are often extremely high or low.

During the final 1/8 of every measurement period, the RATE-OF-CHANGE (i.e., Δ) output indicates zero while the SAMPLE/HOLD module prepares for a data update. This Δ output characteristic can be used to verify sample period duration as well as provide an early indication that data will be updated.

Operator control of ODM measurement cycles is obtained by placing the MODE switch in the MANUAL MODE position. In this mode, the STATUS switch indication will change from SAMPLE to READ when the measurement cycle ends. Momentarily depressing the STATUS switch or placing the MODE switch in the AUTOMATIC mode position will initiate another measurement cycle. Depressing the STATUS switch will have no effect on instrument operation when the switch indicates SAMPLE.

Setting of the SAMPLE TIME-BINARY switch should be changed only when the STATUS switch indicates READ, which will occur only at the end of the sample period when the MODE switch is in the MANUAL MODE position.

4.4 ODM CALIBRATION

The ODM systems are calibrated with MIL-L-7808 oil containing known iron masses. Each mass is measured gravimetrically to an accuracy of 0.1 mg with a single-pan analytical balance. Dissolved iron masses are established with ferrocene. This organo-metallic compound has a 30% weight fraction of iron. Its molecular formula is $FeC_{10}H_{10}$; it is readily dissolved in the oil. All calibrations of concentration levels were performed with ferrocene under static condition.

Settings of the WINDOW BASE and WIDTH are accomplished with ancillary electronic units routinely used in nuclear physics measurements. The analog pulses from the discriminator module are routed through a delay amplifier (1.5 µsec delay) and into

63

a multichannel pulse height analyzer (MCA). The ODM's PHA output is routed through a shaping amplifier and into the MCA to provide a coincidence response with the analog pulses. In this manner the MCA records only the pulse amplitudes (i.e., detected photon energies) which are within the ODM's electronic PHA window. The exact setting is dependent upon the detector's energy resolution; typically the resolution is 20% FWHM. A very large iron mass is commonly used for this operation to negate the effects of background and to expedite instrument adjustments.

After the WINDOW BASE and WIDTH are set, the DISPLAY ZERO potentiometer is adjusted to provide an ODM output indication of zero with the flow-cell containing clean oil. The clean oil is then replaced by an oil sample which contains an iron mass concentration of 200 ppm. The DISPLAY GAIN potentiometer is subsequently adjusted to provide an ODM output indication of full-scale. When the DISPLAY ZERO and GAIN are set, the SAMPLE TIME-BINARY switch is set to give measurement periods of 40 minutes. This is done to obtain the best possible statistical accuracy. Duplicate and triplicate measurements are often made during the calibration sequence to further minimize the statistical uncertainty associated with the settings of DISPLAY ZERO and GAIN.

4.5 DATA INTERPRETATION

The ODM is factory-adjusted to indicate iron contamination ranging from 0 to 80 micrograms (0-200 ppm) and contamination changes from -40 through +40 micrograms (-100 - +100 ppm). These values are indicated as 0 to 1 mA and -500 to +500 µA on the PPM and Δ panel meters, respectively. The PPM and Δ output terminals present voltage levels from 0 to 1 volt, respectively, and -1 to +1 volt, respectively.

Contamination level output is proportional to iron mass detected, measurement time interval and fluid flow rate through the ODM flow-cell. Under static conditions or a constant system contamination level, the ODM output indication will remain constant (within its statistical limits) regardless of SAMPLE TIME-BINARY setting. Consider a case where a prompt step change in contamination occurred and the fluid flow rate through the cell provided a rapid oil volume exchange (on the order of seconds). At the end of the ODM's measurement period, the output level would indicate a fraction of the total change in proportion to that fraction of the measurement period after which the contamination level changed.

The volumetric exchange within the ODM flow-cell can be evaluated with the knowledge of the lubrication system flow rate. The exchange rate is 2.7 cubic centimeters per second for a system flow rate of 1 liter per minute. The volumetric exchange is a squared function of system flow rate. If system

flow rate doubles, the volumetric exchange rate increases by a factor of 4. If the flow rate increases by a factor of 3, the volumetric exchange rate increases by a factor of 9. By comparing the volumetric exchange rate to the total flow-cell volume (160 cubic centimeters), one can evaluate the time period required for a complete exchange of the sample volume.

4.6 SYSTEM TESTS

Tests were performed on each of the ODMs to confirm system accuracy, sensitivity and response as a function of oil temperature. Both static and dynamic testing were conducted to verify system performance characteristics. Some of these characteristics have been discussed elsewhere in this document (i.e., Sections 3.4 and 3.5, Oil Flow-Cell and Temperature Effects, respectively). The measurements related to the sample volume exchange rate tests were obviously performed under conditions of fluid flow; however, the remainder of those tests described in Sections 3.4 and 3.5 were performed under static conditions. Additional measurements are described within this section.

Test hardware, configuration and sequences were incorporated into the overall system performance study. Figure 34 is a schematic representation of the ODM system test loop. A rheostat-controlled centrifigal pump provided the means for oil circulation. Fluid temperature and contaminant-oil mixture uniformity were obtained through use of a laboratory hotplate which had a magnetically-coupled stirrer motor. A pulse counter was used to register the detected count rate in the Fe X-ray window; this pulse signal is outputted from the discriminator board and routed to a standard coaxial cable connector. The same counter was also used periodically to measure the ODM primary clock frequency as derived from the temperature-controlled VFC output. VDC levels from ODM remote output terminals were routed to digital voltmeters; outputs were also periodically presented as strip-chart recorder data.

Contamination levels for system testing were obtained in a manner like that described in the previous section (Section 4.4, ODM Calibration). Baseline data were obtained with clean MIL-L-7808 oil. Volume and temperature measurements established the initial oil mass. Initial dissolved iron concentrations (200 ppm) were obtained by adding known masses of ferrocene. By volumetric dilution with uncontaminated oil stock, subsequent lower iron concentrations were measured. A major portion of the system tests were performed while maintaining a nominal oil temperature of 100°F. Measurements were also taken at oil temperatures of 200°-300°F. The format used for data accumulation and contamination level evaluation is presented as Figures 35(a) and (b). These test sheets provided a logical

65
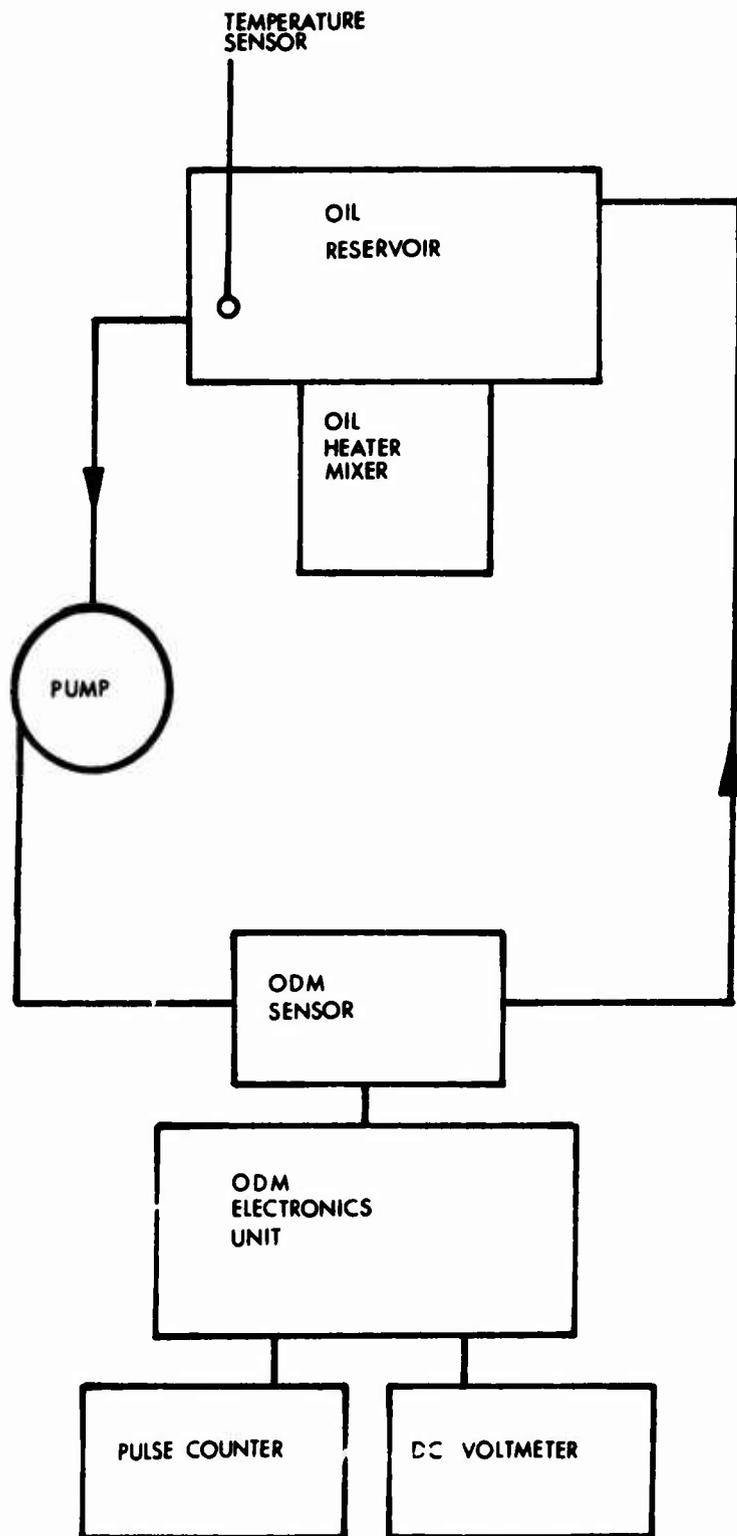
Figure 34. ODM Test Loop.

66

Test #_____   Model 003 - _____

Start time_____   Date_____   Test Operator_____

INITIAL CONTAMINATION (C_o)_____ppm in (M_o)_____ g oil

(Datum transferred from Test #_____DATA ANALYSIS WORKSHEET

Sample volume removed (V_1),_____ml @ (T_1)_____^oF

Clean oil added (V_2)_____ml @ (T_2)_____^oF

ODM Outputs/Test Data @ _____^oF

Time Control Settings,_____BINARY_____DECADE

	Clock Time	RECORDER ppm	Δ	METER ppm	Δ	^oF
1						
2						
3						
4						
5						

NOTES/Ancillary Data

Counting Rate_____

Figure 35(a). System Data Accumulation Format.

67

Test #_____   Model 003-_____

Oil density = 0.955 g cm^{-3} at 37°F (T_o)

α= 4.5 X 10^{-4} per $^\circ$F.

$$\text{Oil mass removed} = \frac{(V_1)\ (0.955)\ (1 + \alpha\ T_o)}{(1 + \alpha\ T_1)} = \underline{\hspace{2cm}}$$

$$M_r = \underline{\hspace{1cm}} g$$

$$\text{Oil mass added} = \frac{(V_2)\ (0.955)\ (1 + \alpha\ T_o)}{(1 + \alpha\ T_2)} = \underline{\hspace{2cm}}$$

$$M_a = \underline{\hspace{1cm}} g$$

$$\text{Final oil mass } (M_f) = M_o - M_r + M_a$$

$$M_f = \underline{\hspace{2cm}} g \quad (M_o \text{ for next test})$$

$$\text{Final contamination } (C_f) = \frac{(C_o)\ (M_o - M_r)}{M_f}$$

$$C_f = \underline{\hspace{3cm}} \text{ ppm iron } (C_o \text{ for next test})$$

ODM Output Evaluation

Effective Count Accumulation = _____cps X _____sec = _____,σ=_____

	(PPM) Recorder (Δ)		(PPM) Meter (Δ)	
Arithemetic mean	_____	_____	_____	_____
Avg. variation	_____	_____	_____	_____

$$\bar{V},\ \text{ppm}/C_f = \underline{\hspace{2cm}} \text{ Vdc per ppm}$$

Figure 35(b). System Data Accumulation Format.

sequential compilation of system test data and an effective record for post-test data analysis.

The primary output data were considered to be those obtained from the remote output terminals. The digital voltmeter (DVM) readings offered greater precision and were more objective than the ODM's analog output meter indications. There was essentially no difference between the mean DVM and analog meter indications. The magnitude of difference can be seen in Table III by comparing the mean value readings with the DVM (i.e., Remote) to those with the analog panel meter (i.e., Meter).

Table III presents a group of typical ODM output data at various concentrations with the test loop operating (i.e., fluid flow conditions). The RMS difference between mean observed values (Remote) and the actual values was calculated to be 3.2 ppm. The count rate statistics associated with mean observed concentration value was equivalent to 4.6 ppm at 1σ. The data are presented in graphic form in Figure 36. The RMS value for the rate-of-change data (Remote Δ) was calculated to be 7.4 ppm; this is equivalent to 1.6σ.

The data of Table IV show long-term reproducibility of ODM measurements. These data show a difference of 12 ppm between the two extremes.

The effects which oil temperature exerts upon ODM performance may be seen in the data of Table V. The trend and its magnitude are reasonably consistent with the data presented in Section 3.5 (Temperature Effects). The data of Table V generally indicate gauging error to be approximately 4 ppm in the positive direction for each $100^\circ F$ increase.

Data scatter distributions are presented in the histographs of Figure 37(a) and (b). The data in the (a) portion is from a sample population (N) of 51 consecutive data with 11-minute sample times, while that in (b) is from an N of 17 consecutive 5.5-minute sample data. The RMS variation was 5.29 ppm of the largest population and longer sample time (Figure 37(a)); the count rate σ was 4.73 ppm. Hence, the RMS variation was equivalent to 1.12σ. The data of Figure 37(b) yielded an RMS variation of 7.82 ppm with a count rate σ of 6.73 ppm. Thus, the RMS variation was equivalent to 1.16σ. The better data grouping of Figure 37(a) is indicative of improved count rate statistics associated with the longer sample time.

The background count rate in the iron X-ray window of the first ODM (Serial No. 01) measured 45.76 counts per second (cps), and the X-ray conversion yield was 0.578 cps for 10 ppm contamination. The X-ray count rates of the second unit (Serial No. 02)

69

TABLE III. MEAN ODM OUTPUT VALUES

Actual Concentration	PPM		Δ	
	Remote	Meter	Remote	Meter
198.9	197.8	199.2	4.4	4.4
149.9	149.6	149.8	8.5	8.4
98.2	101.2	101.0	5.4	5.4
68.9	73.6	71.6	12.4	11.6
52.2	56.8	55.2	4.4	3.4
24.4	21.7	21.7	6.1	7.4

TABLE IV. ODM OUTPUT - WITH TIME VARIATIONS

Date	Normalized to a Constant Concentration of 100 ppm	
	ODM Output (Remote)	ODM Output (Meter)
4-9	110.7 ppm	110.0 ppm
4-12	103.1 ppm	102.9 ppm
4-24	110.5 ppm	111.3 ppm
4-26	100.0 ppm	99.3 ppm

TABLE V. TEMPERATURE EFFECTS

Concentration	ODM Outputs		Temperature
	PPM	Δ	
100 ppm	103.1	5.4	100°F
100 ppm	107.5	15.6	200°F
50 ppm	54.4	4.4	100°F
50 ppm	51.0	13.3	200°F
50 ppm	60.3	14.2	300°F
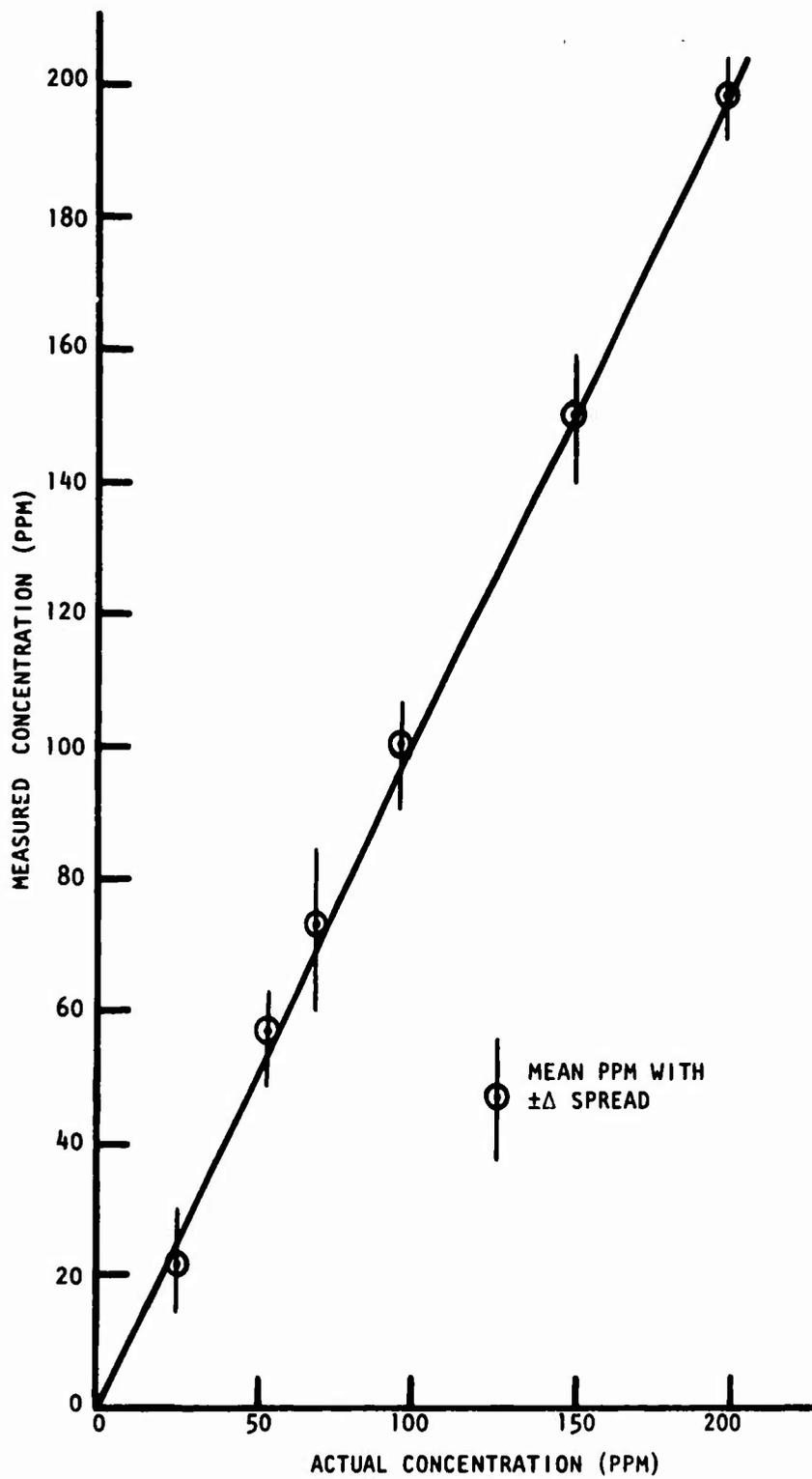
Figure 36. ODM Output Data.
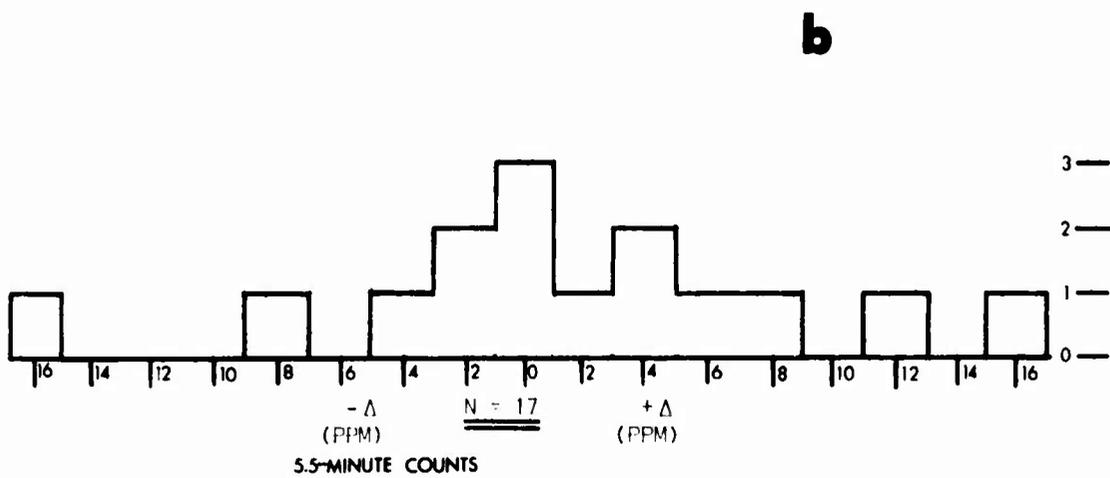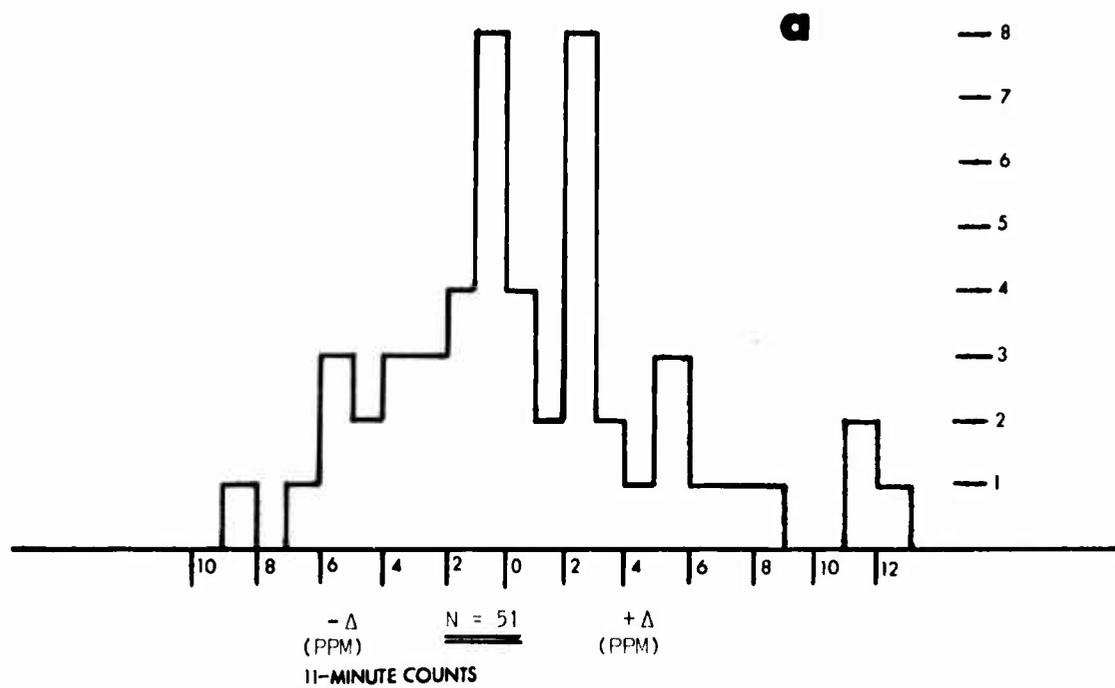
Figure 37. Data Scatter Distributions.

were approximately two times larger (e.g., 91.62 cps background and 1.15 cps per 10 ppm contamination). The differences in detected rates are predominantly caused by differences in source activity (e.g., No. 02 has three times the Pu-238 activity) and detector fill gas (e.g., No. 01 has 2 atm of $Xe-CO_2$ and No. 02 has 2 atm of $Ar-CO_2$).

Although there was no discernible difference between equilibrium dynamic and static test conditions with iron in solution, dynamic testing of the ODM units was unsatisfactory with particulate iron contamination. It was impossible to keep the particles in suspension and yet present a representative oil sample to the ODM flow-cell. The magnetically-coupled stirrer attracted the particles when it was employed; the particles did not stay in suspension without the fluid agitation provided by the stirrer. Static testing with particulate iron yielded results which were consistent with the data presented for iron in solution. Iron X-ray self-absorption was observed when large particles were used. For example, the count rate per gram from a single 122-μm-diameter particle was 36% greater than that produced from a single 630-μm-diameter particle. However, self-absorption did not significantly affect ODM response as a function of mass with particles less than 500 μm diameter.

4.7 DISCUSSION OF ODM PERFORMANCE

The combination of component and system tests demonstrated the performance capability of the ODM. The units permit reasonable latitude in test cell parameters such as lubricant flow rate, temperature, sample measurement times, visual and remote read-out capability, manual and automatic measurement sequencing, etc.

The ODM's 2σ accuracy of ±10 ppm does not match that of the previous laboratory unit, which demonstrated a 2σ accuracy of ±5 ppm. The major reasons for the differences are the increase in background count rate and reduction in detected photon yield.

The ODM background is approximately a factor of 4 greater than the laboratory unit. The factors contributing to the ODM background have been detailed in prior sections of this report. The laboratory unit had a 1-mil-thick plastic window on a polyvinyl chloride oil sample holder; there was no cover on the holder. The masses of scatter material were minimized.

The ODM's detected photon yield is approximately 75% of that obtained with the laboratory unit. As discussed in Section 3.2 (Radiation Detector), the reduction in yield can be attributed to the reduction in detector window area.

Significant effort has been directed toward the development of an ODM in which the instrumental variables are limited, controlled, or known to respond in a predictable fashion. The ODM performance in system tests shows that a major portion of this effort was successful. The greatest remaining factor of uncertainty is that of proportional counter tube aging and/or premature mortality. Performance screening tests, burn-in periods, etc., reduce the probability of accelerated tube performance degradation to an acceptable minimum. Unfortunately, there is presently no way to obtain information "before-the-fact" that will provide absolute assurance that a given detector will last for a lifetime of observing 10^{14} total events.

5.0   POSSIBLE FUTURE PROGRAM CONSIDERATIONS

Detailed data on oil contaminant rate of changes is not available at present. The ODM is intended to contribute information in studies of the relationship between component stress/failure and the metallic contamination in the lubricant. Field tests with the ODM will give insight in areas where measurement needs are not consistent with gauge performance. At that point, consideration can be given to updating the ODM design.

The ODM's size, sensitivity, and simplicity of operation are strong factors in considering the use of the XRF technique for measuring the lubricant quality of used oil samples taken from operational aircraft. Measurements could be routinely made by ground crew personnel as part of the post-flight checkout procedure. The only significant ODM design change necessary for this type of measurement would involve changes in the sample volume configuration.

There was no attempt to make the ODM flightworthy during the performance of this program. However, such a unit is technically feasible. The major problem area in the use of XRF for in-flight measurements is development of a suitable excitation photon source. The use of Kr-85 is considered to be technically inappropriate; however, alternate sources can be considered. Recent advances in the development of small, highly-stable X-ray tubes may provide an effective alternate to the radioactive sources used to date.

Another aspect of in-flight gauging involves improvements in lubricant examination. The measurement time lag, size, and pressure restriction of the present ODM flow cell make it unsuitable for in-flight measurements. An alternative to the flow cell could be to replace a small section of the oil line with a section of beryllium tubing which has been machined in the manner illustrated in Figure 37. A nationally recognized beryllium fabrication facility has given assurance that fabrication of such a configuration is totally feasible.

A stainless-steel tube configuration similar to that shown in Figure 38 was fabricated for a space application[9]. It successfully withstood a pressure differential of 750 psi across the machined window surfaces, which were 0.0015 inch thick.

The key factor which limits performance of the ODM is that of signal-to-noise. Future efforts in ODM development should involve reduction of contamination in the sensor head hardware and further optimization of sensor geometry. The excitation photon intensity and spectral purity available with the aforementioned X-ray tubes appear to offer very promising possibilities in future XRF applications like the ODM.

TYP. 0.01" RADIUS   MATERIAL—BERYLLIUM,
                                                HIGH PURITY
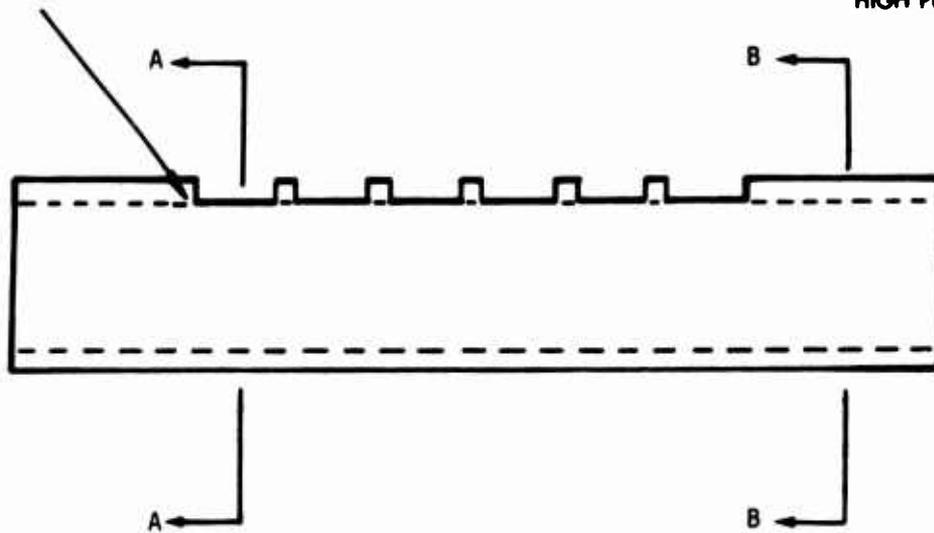
THICKNESS ≤ 0.005"
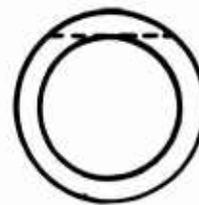
A-A VIEW   B-B VIEW

SCALE 1:1

Figure 38(a).   Flow Tube.

76

WINDOW AREA=2.5" X 0.2
=3.2 cm²
0.2"HAS Xness ⩽15mil

A-A VIEW
SCALE 10:1

Figure 38(b). Flow Tube.

REFERENCES

(1)   Bertin, Michael C., A NUCLEONIC SENSOR FOR DETECTING
       METAL IN RECIRCULATING LUBRICATING OIL SYSTEMS,
       Nucleonic Data Systems; USAAMRDL Technical Report
       72-38, Eustis Directorate, U.S. Army Air Mobility
       Research and Development Laboratory, Fort Eustis,
       Virginia, September 1972, AD 752580.

(2)   Pegg, R. E., and Pollock, J. S., RADIOISOTOPES IN THE
       PHYSICAL SCIENCES AND INDUSTRY II, Vienna, 1962, p. 137.

(3)   Bertin, Michael C., Nucleonic Data Systems, internal
       report, 1972.

(4)   RADIOISOTOPE X-RAY FLUORESCENCE SPECTROMETRY, IAEA,
       Vienna, 1970, p. 45.

(5)   Evans, R. D., THE ATOMIC NUCLEUS, McGraw-Hill Book
       Company, Inc., 1955.

(6)   Baumeister, Theodore, MARK'S STANDARD HANDBOOK FOR
       MECHANICAL ENGINEERS, McGraw-Hill Book Company,
       1966, pp. 5-69, 5-70.

(7)   DESIGNING WITH BERYLLIUM, Brush Wellman, Inc.,
       1970, p. 8.

(8)   HANDBOOK OF CHEMISTRY AND PHYSICS, The Chemical
       Rubber Publishing Company, 1962, p. 3191.

(9)   Harman, R. W., RADIOACTIVE-TYPE PROPELLANT LEVEL
       SENSOR FOR A SPACECRAFT APPLICATION (TRW-PLS),
       TRW Systems Report #08712-J001-R0-00-001, 1967,
       pp. 1-3.

LIST OF SYMBOLS

A   ampere

A_w atomic weight

AGC   automatic gain control

A_o orifice area, cm^2

atm   standard atmospheric pressure

B   background count accumulation

C   total count accumulation

cps   counts per second

CW   clockwise

D/A   digital-to-analog

DVM   digital voltmeter

E_m maximum energy

FWHM   full width at half maximum intensity or pulse height

g   grams

g_n gravitational acceleration, cm/sec^2

HV   high voltage

I   radiation intensity, e.g., $photons/cm^2/sec$

k   empirical factor

kev   thousand electron volts

l   liter

MCA   multi-channel pulse height analyzer

mg   milligram

Mev   million electron volts

N	sample population
ODM	oil debris monitor
p	pressure, psi, g/cm^2 or $dynes/cm^2$
PHA	pulse height analyzer
ppm	parts per million
Q	flow rate, cm^3/sec
R	port radius, cm
r	length
RMS	root mean square
S	contaminant count accumulation
S_m	maximum stress psi
t	thick, in.
T	tube wall thickness, cm
V	volts
v	volume exchange rate, cm^3/sec
VFC	voltage-to-frequency converter
W	load force, psi
XRF	X-ray fluorescence
Z	atomic number
β	ratio of orifice diameter to tube diameter
Δ	used to indicate a variation of uncertainty, e.g., ΔC
η	coefficient of fluid viscosity, dyne sec/cm^2
μ	linear absorption coefficient, cm^{-1} or cm^2/g
μm	micron
μ/ρ	mass absorption coefficient, cm^2/g

ρ fluid density, g/cm^3

σ standard deviation

χ material thickness, cm or g/cm^2